Title of dissertation

Carica papaya L. incorporated nanofibrous scaffold as a potential wound dressing

Degree of study

MSc in Nanotechnology for Medicine and Health Care

Date

25th February 2022

i. Abstract

Title of dissertation: Carica papaya L. incorporated nanofibrous scaffold as a potential wound dressing

Degree of study: MSc in Nanotechnology for Medicine and Health Care

Michaelmas Term 2021

Chronic wound care remains an issue of paramount clinical importance, and an area for entrepreneurial development. The fruit and leaves of the Carica papaya Linn tree possess proteolytic enzymes (papain and chymopapain), various phytochemicals including flavonoids, and Vitamin C that confer proteolytic, antioxidant, anti-inflammatory, and antimicrobial properties, in addition to promoting collagen synthesis. Micro/nano-fibrous dressings mimic the extracellular matrix and promote cellular integration, thus encouraging wound healing and re-epithelialization. Electrospinning is a versatile technique to produce these scaffolds, in which natural and bio-derived synthetic polymers can be utilised. In this experiment, emulsion electrospinning of neat water-in-oil emulsions of sodium alginate (SA) solution and polylactic acid (PLA) in chloroform, using Span60 surfactant, was undertaken. The obtained scaffolds were immersed in $CaCl_2$ solution to convert soluble SA to insoluble calcium alginate (CA). Uniform smooth micro-fibrous scaffolds (diameters ≤ 0.5 μm) were observed on optical microscopy. Attempts to produce bead-on-string fibres through replacement of Na^+ with Ca^{2+} in alginate prior to electrospinning were inconclusive. An aqueous extract of papaya

leaves, seeds, and epicarp was obtained; and incorporated into the emulsions prior to electrospinning. It was discovered that our papaya extract contained Ca^{2+} (measured at 1.16 $mmol.L^{-1}$) and produced insoluble CA when combined with the alginate solution prior to emulsification. This prevented creation of a homogeneous emulsion with ≤ 1.0 mm firm papaya-incorporated CA globules clogging the needle during electrospinning. Thus, papaya extract was added to the SA-PLA emulsion just prior to electrospinning producing a more uniform emulsion which electrospun without clogging. This papaya-functionalised CA-PLA electrospun scaffold had fibres with diameters of 0.5–2 μm, however its gross structure as a membrane was fragile and tore easily (in comparison to neat CA-PLA scaffolds). This is promising evidence that papaya-functionalised CA-PLA electrospun scaffolds can be generated, but optimisation of the technique is still needed.

ii. Table of contents

I. ABSTRACT **1**

II. TABLE OF CONTENTS **3**

III. LIST OF FIGURES **6**

IV. ABBREVIATIONS **8**

V. ACKNOWLEDGEMENTS **9**

VI. DEDICATION **10**

1. INTRODUCTION **11**

1.1 Burden of chronic wounds in Trinidad and Tobago 11

1.2 Electrospinning in Trinidad and Tobago 11

2. BACKGROUND **13**

2.1 Anatomy of the skin 13

2.2 Physiology of wound healing 15

2.3 Pathophysiology of chronic wounds 17

2.4 Carica papaya L. – a natural agent that promotes wound healing 20

2.5 Wound dressings 26

2.6 Micro/nano-fibrous scaffolds as wound dressings 28

2.7 Electrospinning of micro/nanofibers 31

2.8 Electrospinning techniques 39

2.9 Solvent choices for electrospinning 43

2.10 Polymer choices for electrospinning 45

2.11 Functionalization of electrospun fibres and different fibre morphologies 49

2.12 PAPAYA-INCORPORATED ELECTROSPUN SCAFFOLDS 58

3. RESEARCH QUESTIONS 63

4. METHODS 64

4.1 EQUIPMENT 64

4.2 MATERIALS 64

4.3 OBTAINING THE PAPAYA EXTRACT 64

4.4 ELECTROSPINNING APPARATUS 65

4.5 PREPARATION OF NEAT CA-PLA SMOOTH FIBRE ELECTROSPUN SCAFFOLDS 66

4.6 PREPARATION OF NEAT CA-PLA BEAD-ON-STRING FIBRE ELECTROSPUN SCAFFOLDS 67

4.7 PREPARATION OF PAPAYA-FUNCTIONALISED CA-PLA SMOOTH FIBRE ELECTROSPUN SCAFFOLDS (USING $CaCl_2$) 67

4.8 PREPARATION OF PAPAYA-FUNCTIONALISED CA-PLA BEAD-ON-STRING FIBRE ELECTROSPUN SCAFFOLDS (USING $CaCl_2$) 68

4.9 ANALYSIS OF PAPAYA EXTRACT FOR CALCIUM 68

4.10 PREPARATION OF PAPAYA-FUNCTIONALISED CA-PLA ELECTROSPUN SCAFFOLDS (WITHOUT USE OF $CaCl_2$) 68

4.11 PHYSICAL AND MORPHOLOGICAL ASSESSMENT OF ELECTROSPUN SCAFFOLDS 69

5. RESULTS AND DISCUSSION 70

5.1 PREPARATION OF EMULSIONS AND ELECTROSPINNING PROCESS 70

5.2 IMPACT OF PAPAYA ON ALGINATE-PLA EMULSION 72

5.3 GROSS APPEARANCE OF ELECTROSPUN SCAFFOLDS 74

5.4 MICROSCOPIC MORPHOLOGY OF ELECTROSPUN SCAFFOLDS 76

5.5 FUTURE WORK AND RECOMMENDATIONS 82

6. CONCLUSION 84

7. REFERENCES.....86

iii. List of figures

Figure 1: Structure of skin (taken from Junqueira (2010)). 15

Figure 2: Physiology of wound healing by first or primary intention, and secondary intention (taken from Kumar (2013)). 17

Figure 3: Common clinical aetiologies of chronic wounds or ulcers (edited from Eming et al. (2014)). 18

Figure 4: Carica papaya L. (Linn) fruit (left) and tree (right). 21

Figure 5: Basic set-up for electrospinning with examples of possible fibre outcomes; namely smooth fibres versus those with bead defects (compiled using images taken from Hu et al. (2014) and Matabola and Moutloali (2013)). 33

Figure 6: SNC BEST™ patented ball-electrospinning technology (still from a video taken from Stellenbosch Nanofiber Company (2017)). 41

Figure 7: A: positively-charged wire rings as auxiliary electrodes to control fibre deposition with a diagram demonstrating convergence of electric field lines; B: negatively-charged parallel wire collectors to collect aligned fibres with a diagram demonstrating electric field lines concentrating into wires (adapted from Deitzel, Kleinmeyer, Hirvonen, et al. (2001); Li et al. (2003); Teo and Ramakrishna (2006)). 42

Figure 8: Fabrication techniques for functionalised electrospun fibres (taken from Azimi et al. (2020)). 55

Figure 9: Overview of the major steps of microencapsulation in fibres by emulsion electrospinning as done by Qi et al. (2006). 57

Figure 10: Basic steps in the soaking method to obtain a plant extract (taken from Fatehi and Abbasi (2020)). 59

Figure 11: Electrospinning apparatus set-up. 66

Figure 12: Electrospinning of neat CA-PLA bead-on-string emulsions. Visible are the flat-ended needle spinneret with attached high-voltage alligator clip, and the Taylor cone with the just visible thin-fibre jet. The external diameter of the needle is 0.9 mm. Images were captured using the 48-megapixel 1.6 μm Quad Pixel camera on a Motorola One Fusion phone. 70

Figure 13: A: 40 mg.mL^{-1} SA and distilled water solution; B: 40 mg.mL^{-1} SA solution using equal parts distilled water and papaya extract, which was used in sections 4.7 and 4.8 of the methodology..... 73

Figure 14: Gross appearance of electrospun scaffolds. Images were captured using the 48-megapixel 1.6 μm Quad Pixel camera on a Motorola One Fusion phone. 75

Figure 15: Microscopic appearance of electrospun scaffolds. Approximate diameters of fibres in the scaffolds are for A: ≤ 0.5 μm; B: ≤ 0.5 μm and 0.5–2 μm; C: 0.5–2 μm; D: 0.5–8 μm; and E: 0.5–2 μm. White arrows in panel B denote possible 'bead' formation. Images were acquired using a 100× oil immersion objective on an Olympus BX43 optical microscope. 78

Figure 16: A: vertical electrospinning arrangement employed by Qi et al. (2006) in which CA beads in the emulsion can fall into the spinneret; B: horizontal electrospinning arrangement used in this study with the possibility of CA beads settling to the base of the syringe. 80

Figure 17: Microscopic appearance of the papaya extract, acquired using a 100× oil immersion objective on an Olympus BX43 microscope. 82

iv. Abbreviations

AOT: sodium bis-2-ethylhexyl sulfosuccinate

BSA: bovine serum albumin

CA: calcium alginate

$CaCl_2$: calcium chloride

DPPH: 1,1-diphenyl-2-picryl-hydrazyl

ECM: extracellular matrix

EDX: energy dispersive X-ray analysis

G: α-L-guluronate

iNOS: inducible nitric oxide synthase

M: 1,4-linked β-D-mannuronate

PBS: phosphate-buffered saline

PHB: poly-3-hydroxy butyrate

PLA: polylactic acid, or poly-L-lactic acid

PVA: polyvinyl alcohol

ROS: reactive oxygen species

SA: sodium alginate

SEM: scanning electron microscopy

v. Acknowledgements

I would like to acknowledge and give thanks to my supervisors both at the University of Oxford and locally in Trinidad and Tobago. Without their assistance and guidance, this work would not have been possible. I would also like to thank the administrative and technical staff both at Oxford and locally who helped me prepare for, complete, and submit this project.

I would also like to give special thanks to my fiancée, my parents, and my brother who supported and assisted me during my preparations, research, and writing of my dissertation. Their understanding and encouragement throughout this process has been indispensable, especially as this project was undertaken during the height of the COVID-19 pandemic.

Finally, I would like to thank God, for guiding me throughout this process, and allowing me to overcome those difficulties that were encountered through the above-mentioned persons in whose company I was fortunately placed in.

vi. Dedication

This thesis is dedicated to my grandparents.

1. Introduction

1.1 Burden of chronic wounds in Trinidad and Tobago

Trinidad and Tobago has a prevalence of diabetes mellitus of 20.5% in the adult population (Government of the Republic of Trinidad and Tobago, 2012). This is expected to increase in the coming years as there is a 51.5% prevalence of overweight and obesity among children aged 6–12 years in Trinidad and Tobago (Rambaran et al., 2021). Many of these diabetic patients are poorly controlled and go on to develop severe complications including foot ulcers. Diabetic foot infections account for approximately 85 million USD of the Government of Trinidad and Tobago healthcare budget (0.4% of the gross domestic product) (Cawich et al., 2014). These patients require frequent re-admissions to hospital for aggressive debridement and intravenous antibiotics; followed by protracted wound care at a primary care level in which a commonly used dressing agent is the honey-based L-Mesitran® (Triticum Exploitatie B.V., The Netherlands) (Triticum, 2012; Vandeputte, 2003). Not only is it imported using foreign exchange, but it is produced using a natural substance. Therefore, Trinidad and Tobago has the potential to earn rather than spend in this market using the ample local resources.

1.2 Electrospinning in Trinidad and Tobago

While electrospinning is a mature field, it is still relatively new to the Caribbean. There are numerous studies on nanotechnology originating from within the region, but only few published articles on the topic of electrospinning. Singh et al. (2018)

of Barbados investigated electrospun fibres of poly-vinyl cinnamate in 1,2-dichloroethane, while the third author in the study on electrospun poly-L-lactic acid (PLA) nanofibers by Ramesh et al. (2020) was from St Kitts and Nevis. Outside of the Anglophone Caribbean, the last author in the article by Gomes et al. (2007) was from Puerto Rico and they looked at electrospinning using of polyacrylonitrile dissolved in N,N-dimethylformamide. Otherwise, and to the best of my knowledge, this appears to be the first attempt at electrospinning in Trinidad and Tobago. This is based not only on a paucity of published articles or grey literature, but also because of a lack of knowledge on the topic across the academic and industrial communities within Trinidad and Tobago. This latter discovery revealed itself while attempts were made 'on the ground' to source equipment for and obtain advice on electrospinning; of which the results were futile. Equipment for use had to be purchased from international suppliers and are now available locally to continue research in this area. This dissertation not only serves to fulfil my requirement for the Master of Science degree, but also serves as a steppingstone to promote and continue research into electrospinning (and nanotechnology) locally.

2. Background

2.1 Anatomy of the skin

Skin is the largest organ of the body, and along with its appendages, forms the primary barrier to the external environment. The skin defends against ultraviolet radiation, physical and chemical agents, as well as pathogenic microorganisms. As a permeability barrier, it also prevents desiccation of the internal environment. Beyond this, the skin plays several other roles: thermoregulation, sensory function (via receptors for touch, vibration, pain, and temperature), synthesis of cholecalciferol, excretion via sweat glands, immunological surveillance, and socio-sexual communication (via appearance and release of pheromones) (Boer et al., 2016; Junqueira, 2010; Sullivan & Myers, 2022).

The skin is comprised of three main layers: epidermis, dermis, and hypodermis or subcutaneous layer (Figure 1). The epidermis is a stratified keratinised squamous epithelium arranged in five layers from deep to superficial: stratum basale or germinative layer, stratum spinosum, stratum granulosum, stratum lucidum, and stratum corneum. These strata demonstrate progressive proliferation, differentiation, and maturation of keratinocytes from deep to superficial. The cornified layer consists of flattened, unnucleated, fully keratinised cells which are arranged in a brick-and-mortar pattern in a lipid-rich intercellular matrix and are continuously shed from the surface. The epidermis also contains pigment-producing melanocytes, antigen-presenting Langerhans cells, and sensory Merkel cells. The dermo-epidermal junction is formed by a basement membrane which

follows the contours of the interdigitations between the dermal papillae and epidermal ridges. The basement membrane also supports the avascular epidermis. The dermis is a layer of irregular, fibroelastic connective tissue giving skin its tensile and mechanical strength. It is comprised mainly of interwoven type I and type III collagen fibres with other components of extracellular matrix (ECM) including glycosaminoglycans like hyaluronic acid and dermatan sulphate, and elastin fibres. The dermis is split into the superficial papillary and deep reticular dermis. The former is more loose connective tissue with a greater density of fibroblasts, macrophages, and mast cells. The reticular dermis is thicker, less cellular, and more tightly packed with collagen fibres. There is a subpapillary plexus of blood vessels at the division of the papillary and reticular layers, and the dermis has a complex lymphatic and nerve network. The subcutaneous layer or hypodermis consists of loose connective tissue with a high proportion of fat cells, that binds skin loosely to the deeper organs, allowing the skin to slide over them. It has a rich vascular supply. The skin appendages like hair follicles, sweat and sebaceous glands pass through the dermis and may extend into the underlying subcutaneous fat (Boer et al., 2016; Junqueira, 2010; Sullivan & Myers, 2022).

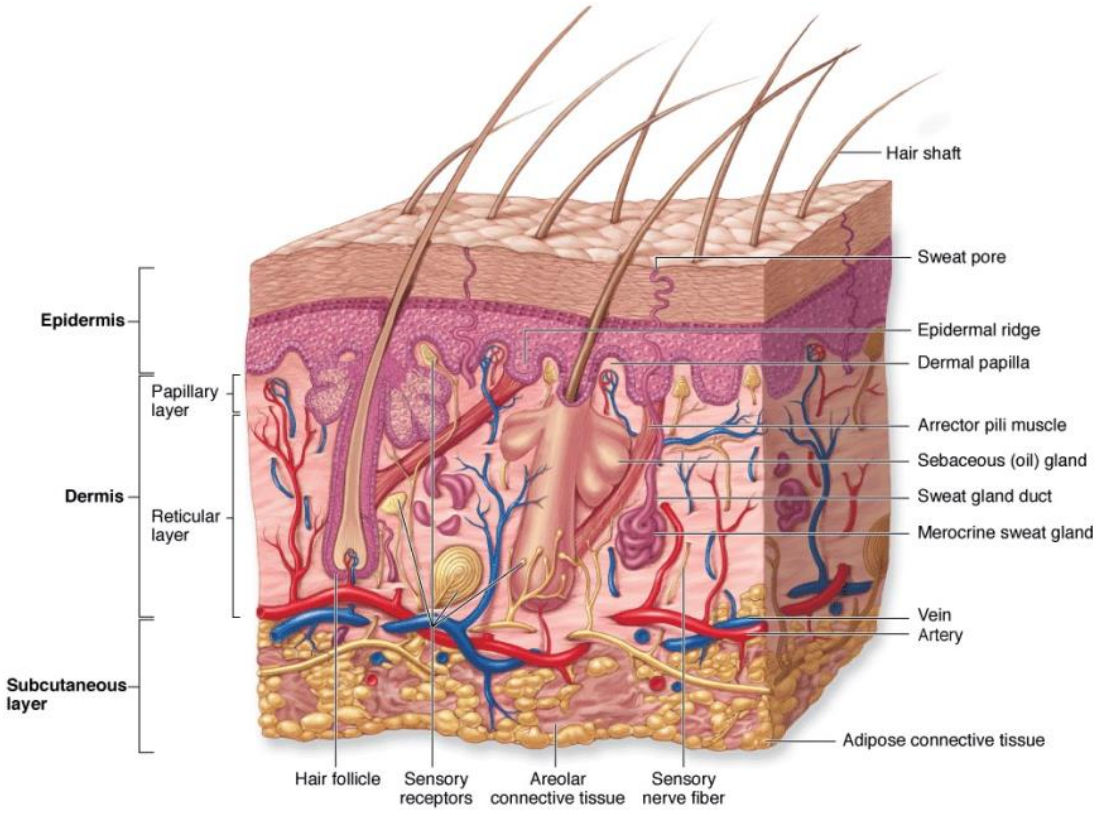


Figure 1: Structure of skin (taken from Junqueira (2010)).

2.2 Physiology of wound healing

Healing of cutaneous wounds occurs via a combination of epithelial tissue regeneration and formation of connective scar tissue. It usually follows four overlapping phases of haemostasis, inflammation, proliferation, and remodelling. Haemostasis occurs immediately to limit blood loss and is characterised by platelet clot formation which provides a temporary matrix for cell migration. The inflammatory phase follows shortly after and lasts 3–4 days post-injury. Platelets secrete growth factors and cytokines causing capillary leak and an influx of inflammatory cells which result in the clinical hallmarks of erythema, swelling, warmth, pain, and loss of function. The predominant cell types are phagocytic cells

which aim to clear bacterial contamination, foreign material, and cellular debris. Neutrophils also produce reactive oxygen species against pathogens, and proteases to degrade tissue debris. Monocytes that arrive to the wound site differentiate into tissue macrophages, which in addition to the above also secrete various growth factors and cytokines which recruit fibroblasts, endothelial cells, and keratinocytes to begin repair. There is then apoptosis of the immune cells, and wound healing now enters the proliferative phase which lasts from 4–28 days. Fibroblasts produce type III collagen and hydrated glycosaminoglycans or ground substance which act as a tissue scaffold to replace the area of dermal loss. This uncovered tissue appears as granulation tissue within which endothelial cells grow rapidly in angiogenesis. Re-epithelisation occurs from the edges with keratinocyte proliferation until the wound is fully covered. The final stage is remodelling which can last up to 1–2 years and is characterised by organisation of the provisional tissue matrix. The type III collagen is replaced by type I collagen and the structure becomes lamellar and cross-linked. Fibroblasts mature into myofibroblasts which aid in wound contraction, and there is vascular regression. There is return of some normal structure, however the tissue only reaches 70–80% of its pre-injured maximum tensile strength. Based on the size and nature of the cutaneous injury, wound healing can be said to occur by primary or secondary intention (Figure 2). Primary intention occurs in clean, uninfected wounds that are usually approximated by sutures. There is only focal disruption in the dermo-epithelial basement membrane, and healing is primarily by epithelial regeneration with minimal scar tissue formation and wound contraction. Secondary intention occurs in wounds that have a greater volume of tissue loss and are more complex or infected. It follows the same four phases of wound healing outlined previously, and the greater volume of

granulation tissue results in more scar tissue formation compared to epithelial regeneration (Frykberg & Banks, 2015; Han & Ceilley, 2017; Kumar, 2013; Sullivan & Myers, 2022).

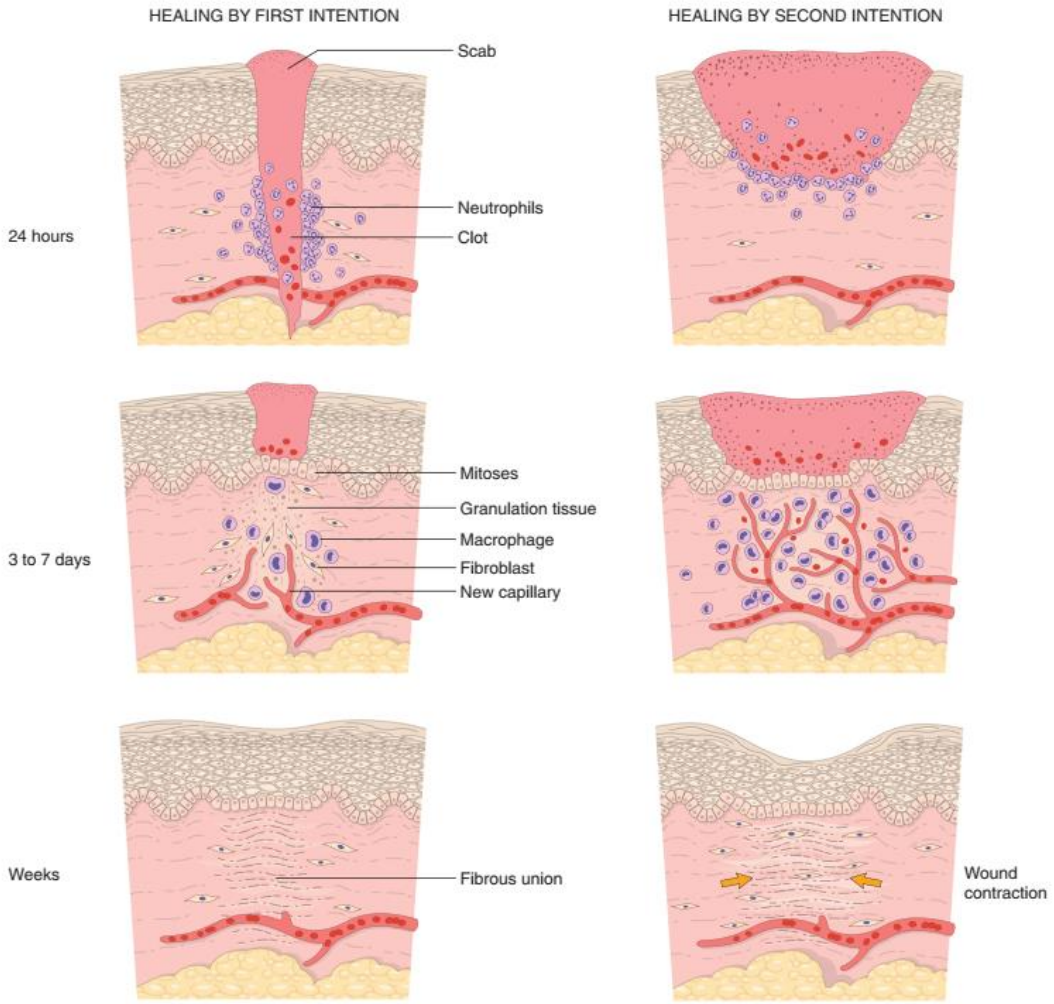


Figure 2: Physiology of wound healing by first or primary intention, and secondary intention (taken from Kumar (2013)).

2.3 Pathophysiology of chronic wounds

Chronic wounds are ulcerative skin defects that fail to re-epithelialize and progress through the normal stages of wound healing. The most chronic wounds usually

occur in the lower limbs and are classified based on their clinical aetiology: chronic venous insufficiency, ischaemia from atherosclerosis and peripheral arterial disease, diabetic ulcers which have neuropathic and vasculo-pathic components, and pressure decubitus ulcers (Figure 3). Additionally, systemic factors contribute to poor wound healing such as advanced age, nutritional impairment, compromised immune function, certain medications, and metabolic disease or comorbidities (Eming et al., 2014; Frykberg & Banks, 2015).



Figure 3: Common clinical aetiologies of chronic wounds or ulcers (edited from Eming et al. (2014)).

Chronic wounds share a similar molecular pathophysiology often arresting in the inflammatory phase of wound healing. There is a constant influx of immune cells due to repeated tissue injury, the presence of microbes and platelet-derived growth factors. This leads to amplification of the cytokine cascade (including interleukin-1β and tumour necrosis factor–α) which in turn leads to elevated levels of proteases. In normal wound healing, protease levels are closely balanced by

corresponding inhibitors; but in chronic wounds they become in excess causing destruction of ECM thus preventing progression to the proliferative phase of wound healing (Frykberg & Banks, 2015; McCarty & Percival, 2013).

All the degraded ECM further stimulates migration of inflammatory cells to the wound site. This build-up of necrotic debris firstly serves as a growth medium for pathogens and formation of a biofilm. A major role of the inflammatory phase of wound healing is to curb microbial growth, and the presence of infection serves to initiate and maintain chronic wounds. The necrotic debris is also worsened by low (≤ 5 mmHg) oxygen tensions in chronic wounds. An oxygen tension of at least 20 mmHg is needed in wound healing to supply dividing cells, interact with cytokines, and feed the neutrophil respiratory burst. The persistent inflammatory and hypoxic state also results in immune cells producing excess reactive oxygen species (ROS) causing cell and ECM damage, and further stimulation of cytokines and proteases. Furthermore, in diabetic wounds, there are elevated levels of advanced glycation end-products which exacerbate oxidative stress and disrupt normal physiological function (Eming et al., 2014; Han & Ceilley, 2017; Hunt & Hopf, 1997; Rajendran et al., 2018; Sheffield, 1988).

Cell populations in chronic wounds (such as fibroblasts, keratinocytes, and endothelial cells) are also senescent, proliferate inadequately and respond poorly to wound healing signals. It is possible that oxidative stress from the inflammatory state and ROS leads to metabolic changes, and nucleic acid damage with resultant impairment of the normal cell cycle. As such, keratinocytes are non-migratory, and the wounds do not re-epithelialize. Furthermore, stem cell populations locally in

the wound bed, and systemically may be compromised and depleted in patients with chronic wounds (Schultz et al., 2003; Stanley & Osler, 2001; Telgenhoff & Shroot, 2005).

Inadequate angiogenesis in chronic wounds can result from proteolytic degradation of proangiogenic factors, presence of antiangiogenic proteins (e.g., myeloperoxidase in diabetic wounds) and endothelial cell senescence. The decreased blood vessel growth can deprive the wound of nutrition and oxygen needed for healing. Additionally, in chronic wounds there may deficiencies of protein, zinc, vitamins A, C, and E; all of which are needed in either ECM and collagen formation, or proper immune function (Galeano et al., 2001; Krisp et al., 2013; Lauer et al., 2000; MacKay & Miller).

2.4 Carica papaya L. – a natural agent that promotes wound healing

Carica papaya L. (Linn) (Figure 4) commonly referred to as papaya or pawpaw is a fruit-bearing, soft-wooded, unbranching tree which is native to the north-tropical Western hemisphere. It is cultivated for consumption in Trinidad and Tobago, with fruits hanging from stalks attached to the upper trunk of the tree. Of note, all parts of the papaya plant, especially the unripe fruit, contain a white, bitter, liquid latex (OECD, 2005).



Figure 4: Carica papaya L. (Linn) fruit (left) and tree (right).

Papaya has traditionally been used as a topical agent for various skin disorders and wounds. It possesses antioxidant, anti-microbial, anti-inflammatory/immunomodulatory, and proteolytic properties, the latter making it also well known in the culinary environment as a meat tenderizer. Papain and chymopapain, present in various parts of the papaya plant and fruit, are the proteolytic enzymes which can be used for debridement of sloughy or necrotic wounds. Jayarajan et al. (2016) demonstrated that this proteolytic activity was preserved after autoclaving when they used unripe papaya pulp in second- and third-degree burn victims. Vasuki et al. (2017) and Murthy et al. (2012) both found papaya dressings to be effective debridement agents with faster times to granulation, when compared to mechanical debridement via wet-to-dry saline or hydrogen peroxide dressings respectively, for infected diabetic ulcers or surgical site dehiscence. As mentioned in section 2.3, protease activity in wound healing should be closely balanced so that excessive loss of granulation tissue does not

occur. The use of papaya for enzymatic debridement (and in fact, all forms of mechanical and chemical debridement) are closely monitored in wound care so that once the wound is no longer necrotic or sloughy, the agent can be adjusted or withdrawn accordingly. In situations where papaya is left on the wound, proteolytic enzymatic kinetics should be considered in which saturation, inactivation, and protease-on-protease degradation or distraction can attenuate enzymatic debridement as granulation ensues (Ferrall-Fairbanks et al., 2020).

Grated unripe green papaya pulp and latex are used as cheap, effective, and readily available dressings for chronic foot wounds in Trinidad and Tobago, and this use in clinical practice prompted local studies by Nayak et al. (2012; 2007). In the first study, an aqueous extract of unripe papaya epicarp was used in excision and dead space wounds in diabetic rats. The time (mean ± SE) for full re-epithelization in excision wounds treated with papaya extract was 15.1±0.16 days as compared to 15.5±0.2 days in those treated with mupirocin ointment, an antibacterial standard-of-care treatment. While the papaya extract achieved faster wound contraction, it was not statistically significant. There were also greater wet and dry weights of pink healthy granulation tissue (p-value < 0.001) excised from wounds treated with extract as compared to negative controls. Furthermore, there was an approximately 1.5-fold increase in hydroxyproline content (p-value < 0.001) in wounds treated with the extract compared to negative untreated controls. Papaya fruits and leaves contain vitamin C which acts as a co-factor for proline and lysine hydroxylases, with hydroxyproline and hydroxylysine being essential in collagen formation. Vitamin C also activates fibroblast cells to produce more collagen and elastin (Ahlawat et al., 2019; Fatima & Shahid, 2018). Nafiu and Rahman (2015) found that application of

papaya extract to excision wounds in rats leads to an increased nitrite content (of approximately 25 $\mu M.mg^{-1}$ of protein, p-value < 0.05) early on in wound healing as compared to negative controls (approximately 16 $\mu M.mg^{-1}$ of protein), which subsides by around day ten. Nitrite is the stable breakdown product of nitric oxide which in turn is the enzymatic product of inducible nitric oxide synthase (iNOS), thus measurement of nitrite is an indirect measurement of iNOS activity. Nitric oxide derived from iNOS leads to increased expression of vascular endothelial growth factor, angiogenesis, and collagen synthesis. The decrease in nitric oxide production in the later stages of wound healing is beneficial as excess angiogenesis and collagen deposition can lead to abnormal scar tissue.

In the second study by Nayak et al. (2012), an ethanol extract of papaya seeds was used again in excision wound models in rats. This time re-epithelization rates for wounds treated with papaya extract were statistically significantly greater (p-value < 0.001) than the mupirocin dressed wounds. Hydroxyproline content was again increased, and histological analysis confirmed significant collagen deposition and fibroblast activity. Phytochemical analysis was performed to identify potentially active ingredients, and it was suggested that flavonoids have antioxidant properties, while alkaloids like carpaine, glycosides like glucotropaelin, and benzyl-isothiocyanate all have some form of antimicrobial properties. Papaya extract also contains other saponins (glycosides with foam-forming and detergent properties), tannins, and sterols; all of which have either antimicrobial, anti-inflammatory, or antioxidant properties (Dwivedi et al., 2020; Nayak et al., 2012).

Nugroho et al. (2017) found seven flavonoids in papaya leaf extract of which kaempferol 3-(2^G-rhamnosylrutinoside) was the most abundant. Furthermore, they confirmed the antioxidant and free radical scavenging properties of these flavonoids via peroxynitrite-scavenging assays. Extracts from various parts of the papaya tree and flower were confirmed to have antioxidant properties via measuring decreased levels of malondialdehyde (a product of oxidative damage), assessing inhibition of lipid peroxidation, and via the 1,1-diphenyl-2-picryl-hydrazyl (DPPH) free radical scavenging assay (Asghar et al., 2016; Dwivedi et al., 2020; Nafiu & Rahman, 2015). Mikhal'chik et al. (2004) also found that fermented papaya reduced the generation of superoxide, hydroxyl radicals and other ROS in vitro. In vivo, papaya applied to burn and excision wounds in rats also reduced myeloperoxidase activity which converts hydrogen peroxide to hypochlorous acid, and is a measure of polymorphonuclear leucocyte influx (Mikhal'chik et al., 2004; Nafiu & Rahman, 2015). Nafiu and Rahman (2015) utilised the rapid spectrophotometric method for measuring catalase activity, the inhibition of the auto-oxidation of pyrogallol by superoxide dismutase, and a glutathione peroxidase cellular activity assay; and found that unripe papaya pulp extract increased (p-value < 0.05) the activities of catalase (approximately 5.5-fold on day four), superoxide dismutase (approximately 2-fold on day four), and glutathione peroxidase (approximately 1.5-fold on day ten) as compared to negative untreated controls in excision wound beds of rats; thereby demonstrating the ability to quench free radicals in vivo.

Alkaloids, phenolics, carotenoids, and glucosinolates present in papaya have been shown to reduce levels of inflammatory markers including tumour necrosis factor-

α, interferon-γ, several interleukins, and pro-inflammatory cytokines (Pandey et al., 2016). Papaya extract in phosphate-buffered saline (PBS) applied to excision wounds in rats was shown to reduce activity of cyclooxygenase-2 enzyme and its product prostaglandin E2, thus reducing infiltration and activation of inflammatory cells into the wound site (Nafiu & Rahman, 2015). In West Indian in vitro studies, Nayak et al. (2012; 2007) who utilised seed and epicarp extract, and Dawkins et al. (2003) who utilised seed extract, both found antibacterial activity of papaya spanning across the following organisms: B cereus, E coli, S faecalis, S aureus, P vulgaris, S flexneri, P aeruginosa, P murabilis, E agglumerans, and S choleraesuis. In addition to the antimicrobial effects of several of the previously mentioned phytochemicals present in the papaya plant, papain and chymopapain have antimicrobial activity and have been suggested to degrade the debris-rich biofilm in wounds thus allowing adequate tissue oxygenation (Asghar et al., 2016; Dwivedi et al., 2020; Kong et al., 2021; Nayak et al., 2007).

Asghar et al. (2016) compared the medicinally beneficial properties of different extractions (using different organic and aqueous solvents) of papaya roots, bark, seeds, pulp, peels, and leaves. They found that ethanol extraction of the pulp and leaves had excellent antioxidant properties (p-value < 0.001) yielding high DPPH free radical scavenging potentials at 68.07% and 75.05% respectively, as well as the highest linoleic acid peroxidation inhibition at 81% and 85% respectively. Methanol extracts of the same also demonstrated high antioxidant activities. Reducing power was assessed by measuring absorbance of the colour change as Fe^{3+} is reduced to Fe^{2+}. Ethanol, water, and methanol extract of papaya leaves had the highest reducing powers with absorbances of 1.99, 1.87, and 1.57 respectively.

Antibacterial activity was assessed by measuring the zones of inhibition around extract-loaded paper discs on agar cultured with four different bacterial strains. Ethanol extracts of pulp and leaves were the most effective (p-value < 0.05 and < 0.001 respectively) with zones of inhibition ranging 14–18 mm, as compared to other extracts. Methanol was the next best solvent, however all other extracts including water-derived ones produced zones of inhibition of approximately ≤ 12 mm with the majority being < 10 mm. It has been suggested that hydrophobicity is a domain driver of antibacterial activity which is why water performed poorly in that regards. With regards to recognising the presence of papaya extract or any of its constituent phytochemicals, UV-visible spectroscopy was performed on papaya extracts and the spectra of phenolic compounds and flavonoids was found in the ranges of 230–290 nm and 300–350 nm, while the presence of vitamin C was confirmed via a maximum absorbance peak at 255 nm (Ahlawat et al., 2019; Dwivedi et al., 2020).

2.5 Wound dressings

Chronic wounds are usually covered with a sterile dressing material to minimize exogenous contamination and pain, and promote wound healing. Ideal characteristics in a dressing are: i) maintains a moist environment while removing excess exudate; ii) protects wound from further trauma and contaminants; iii) enhances epidermal migration; iv) promotes angiogenesis and connective tissue synthesis; v) allows gaseous exchange and oxygenation; vi) thermally insulating to maintain appropriate tissue temperature; vii) impermeable to bacterial infection; viii) non-adherent to permit removal without causing secondary trauma; ix)

capable of providing debridement action; x) sterile, non-toxic, and non-allergenic; xi) cost effective and long shelf-life; and xii) comfortable, conformable, and requires infrequent changes (Dhivya et al., 2015; Jones et al., 2006).

Traditional wound dressings employ woven gauze (also bandage or cotton wool) either dry or coated with an appropriate solution or ointment. Gauze however tends to adhere to the wound bed and causes secondary trauma, risks maceration of the wound if left unchanged for too long, fails to adequately maintain a moist environment, and disrupts wound healing (Dhivya et al., 2015; Jones et al., 2006). Gauze dressings are scarcely used in the United Kingdom, however their inexpensiveness and availability account for their common use for chronic wounds in Trinidad and Tobago. Other more recent wound dressings are (Dhivya et al., 2015; Jones et al., 2006):

a) low-adherent, open-weave tulle dressings soaked in agents that promote wound healing or are antimicrobial.
b) semi-permeable film dressings. These are transparent to allow ease of inspection, highly flexible and adhesive, and allow transmission of gases. They are impermeable to contamination and bacteria but handle excess wound exudate poorly.
c) semi-permeable foam dressings consist of an inner hydrophilic polymer foam with an outer semi-permeable hydrophobic backing. They are conformable and highly absorbent, suitable for increased exudative output. They provide good protection against external trauma but require frequent changing and are not ideal for drier wound beds as the exudate helps facilitate wound healing.

d) hydrocolloids in which a gel-forming inner colloidal layer is bonded to an external semi-permeable film or foam. An impermeable rehydrating gel is formed over the wound, which is useful for dry necrotic wounds and can promote autolytic debridement. They however do not handle excess exudate well, and do not allow ease of inspection.

e) hydrogels are a matrix of insoluble hydrophilic polymers with a high-water content that ensures a moist wound environment. They are suitable for all stages of wound healing and can facilitate debridement through rehydration and autolysis. While useful for dry or necrotic wounds, they are not suitable for infected wet wounds where the exudative build-up can result in maceration or bacterial proliferation. Hydrogels also have poor mechanical stability.

f) alginate dressings are formed from sodium and calcium salts of seaweed-derived alginic acid. They are good for highly exudative wounds due to extreme absorbent properties, and alginates form a gel with the exudate thus limiting bacterial proliferation. They are not suitable for drier wound beds as they can adhere and cause pain and impairment in healing.

2.6 Micro/nano-fibrous scaffolds as wound dressings

Micro/nano-fibrous scaffolds are usually a non-woven, criss-crossing network of fibres at the micro/nano-sized level. These scaffolds are promising for wound dressing applications due to their characteristic features. The fibrous scaffold closely mimics the ECM which serves as a supporting framework for cellular attachment, proliferation, migration, and differentiation. Native ECM of skin is

comprised of elastin, keratin, and collagen fibres with diameters of 50–500 nm that are cross-linked into a complex, random, porous network. The micro/nano-fibrous scaffolds can be produced using a variety of polymers (as described in section 2.10) which are generally biodegradable. This ensure that the scaffolds only act as a temporary ECM-mimic to recruit cells, which can then proliferate and secrete biomolecules and growth factors to begin construction of permanent native ECM (Abrigo et al., 2014; Stocco et al., 2018; Xue et al., 2019). The fibrous scaffolds have a large surface area-to-volume ratio which improves haemostasis at the wound site and lends itself to functionalisation with drugs or other bio-active molecules (discussed further in section 2.11). There also exists a high interconnected porosity of 60–90% with a variable pore size distribution within the fibrous scaffolds. This micro/nano-sized porosity allows fluid exudation while still preventing wound dehydration and desiccation, permits high oxygen permeation and cellular respiration, and limits bacterial invasion (Abrigo et al., 2014; Azimi et al., 2020; Stocco et al., 2018). However, different tissues require different pore sizes to optimise cellular infiltration, and the optimum pore size for skin growth and wound healing has been stated as being 20–120 μm (Elsner et al., 2012).

Micro/nano-fibrous scaffolds can be produced through several techniques (Stocco et al., 2018):

a) rotary-jet spinning: a polymer solution-containing reservoir with two side-wall orifices rotates at high speed such that a viscous jet is expelled from the orifices under centrifugal forces. This jet takes a coiled trajectory, as the solvent evaporates, onto a cylindrical collector. It has a high production rate

and works with a wide range of polymers and solvents, however there is decreased homogeneity across the fibres.

b) airbrush or blowspinning: a pressurised gas is streamed around a nozzle with the polymer solution, generating fibres in the direction of gas flow. The set-up is relatively cheap and simple, however bundling of fibres occurs.

c) self-assembly or biomineralization: scaffolds form from spontaneous self-assembly of natural or synthetic building blocks (e.g., hydrogels of low-molecular weight gelators, and amyloid fibres from peptides and proteins). Nanofibers of 5–8 nm in diameter can be generated, however their lengths can only reach several micrometres and only certain polymers can be used.

d) phase separation: separation of a polymeric solution into two phases is promoted through cooling or non-solvent exchange. A now immiscible, polymer-rich phase (the eventual scaffold) is formed within the polymer-poor phase (or solvent). The solvent is extracted, and the scaffold frozen to maintain its porous structure. Three-dimensional scaffolds with large pores are formed, however fibre diameter is difficult to control, and only certain polymers can be used.

e) spinneret-based tuneable engineered parameter or STEP technique: micro/nano-fibres are pulled or drawn from a solution droplet onto a substrate sequentially or continuously under high speeds. The absence of electrical instability allows for a collection of highly aligned fibres of uniform dimension and spacing, however it is limited to viscoelastic materials.

f) electrospinning: this is the commonest and most versatile technique to produce scaffolds and will be discussed in detail in the sections below.

2.7 Electrospinning of micro/nanofibers

Electrospinning is an electrohydrodynamic process in which application of an electrostatic force is used to draw continuous fibres from a liquid polymer solution or melt. It is in the 1600s that William Gilbert first recorded deformation of a water droplet in response to an electrostatic field produced by rubbing amber. Over the next few centuries, the discipline saw advancements in industrial spinning processes, and the generation of high-current electricity with sufficient voltage that overcame the limitations associated with triboelectric methods. In 1888, Charles Vernon Boys performed electrospinning using a small, insulated dish connected to a high-voltage electrical supply, and successfully drew fibres from beeswax, shellac, sealing-wax, and collodion melts. These fibres were mechanically ineffective though, and he went on to draw his desired almost nano-scale silica fibres through shooting a heated quartz pellet attached to a crossbow bolt. John Francis Cooley filed the first electrospinning patents in the early 1900s, in which he described apparatus and methods to spin fluids in an electric field generated by a Wimshurst influence generator and collect fibres via reeling onto a glass rod. Advancements in electrospinning continued to be made, most notably with Anton Formhals who filed 22 patents in the mid-20th century, describing various electrospinning configurations (Ghosal et al., 2018; Tucker et al., 2012). Between 1964–1969, Geoffrey Ingram Taylor mathematically modelled the shape of the cone of fluid under the influence of an electric field. This is currently known as the Taylor cone and possesses a semi-vertical angle of approximately 49.3° (Taylor & Van Dyke, 1969; Taylor, 1964; Tucker et al., 2012). Only some of the many persons who contributed to the discipline are mentioned here, and since the 1990s, research and

patent applications regarding electrospinning have continued to increase almost exponentially to the current state of the technology as it is today.

The basic electrospinning setup involves a high-voltage power supply, a syringe with needle spinneret regulated via a syringe pump, and a usually grounded collector as can be seen in Figure 5. As the polymer solution or melt is slowly expelled from the syringe, a semi-spherical droplet of liquid is formed at the needle tip. The high-voltage (usually 5–30 kV) electric field set up between the needle and collector induces charges on the surface of the liquid droplet, resulting in deformation of the droplet into the Taylor cone. As the electric field intensifies and reaches a critical value, the repulsive electric forces overcome the surface tension of the droplet and a charged jet of the liquid is ejected from the tip of the Taylor cone and travels in a spiralling path of increasing diameter towards the collector. In the case of a polymer solution, as the jet travels through the air, the solvent evaporates leaving behind a polymer micro/nanofiber (Hu et al., 2014; Stocco et al., 2018; Taylor & Van Dyke, 1969). Melt electrospinning involves electrospinning directly of the polymer melt (without need for a dissolving solvent). However, the technique is still in its infancy due to very high processing temperatures (which impair its ability to be functionalised), high viscosities, and the inability to attain nanometre fibres. Thus, melt electrospinning will be discussed no further, and all mention of electrospinning will be in reference to polymer solutions (Bhardwaj & Kundu, 2010).

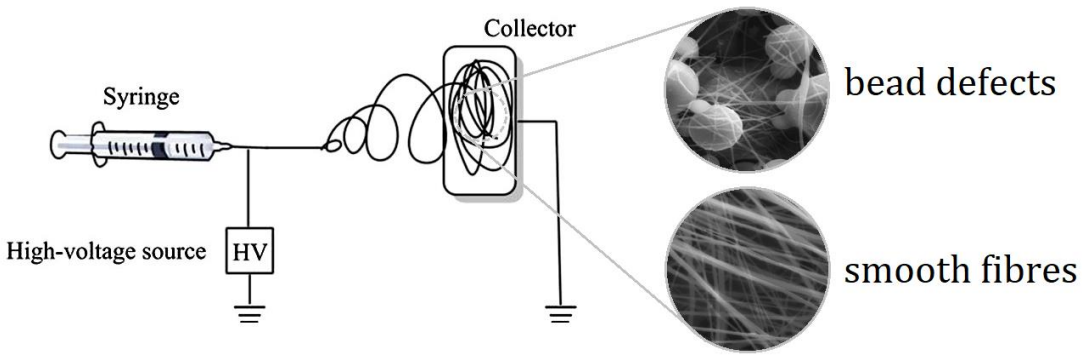


Figure 5: Basic set-up for electrospinning with examples of possible fibre outcomes; namely smooth fibres versus those with bead defects (compiled using images taken from Hu et al. (2014) and Matabola and Moutloali (2013)).

Several parameters have been found to influence the fibres formed during electrospinning:

a) applied voltage or electric field strength: charge is transported via the polymer solution from the charged needle to the grounded target producing a measurable current. An increase in the applied voltage causes an increase in this spinning current, which results in a greater mass flow rate of polymer (Deitzel, Kleinmeyer, Harris, et al., 2001). Deitzel, Kleinmeyer, Harris, et al. (2001) found that for polyethylene oxide/water electrospinning systems, a voltage of 5.5 kV caused initiation of the jet and production of smooth straight fibres, whereas voltages above 7 kV resulted in bead defects in the spun fibres. They found that at voltages of 5.5–7 kV, the jet begins from the Taylor cone of a drop at the needle tip, however at higher voltages the jet originates from at or within the needle tip exceeding the rate at which solution is brought to maintain the Taylor cone. The result is an unstable jet with bead defects. Matabola and Moutloali (2013) found similar with

increasing voltages in polyvinylidene fluoride/N,N-dimethyl acetamide systems. Below 12 kV, the charge density on the surface of the jet was not enough to maintain stability and so large bead defects were formed upon fibres with diameters of ≤ 100 nm. At 14–16 kV, the produced fibres were smooth and of a relatively larger diameter (160–180 nm) likely due to stability associated with the charge density and jet velocity. At 18 kV, multiple jets originated from within the needle tip. This complex phenomenon resulted in smaller fibres with diameters of 150 nm (due to the higher jet velocity) and bead defects, dispersed over a larger surface area as the different fibres repel each due to the flowing charge on their surface (Matabola & Moutloali, 2013; Sousa Coelho et al., 2018).

b) collector: this must be made of a conductive material to maintain the electric field needed for electrospinning. A non-conductive material will negatively affect fibre collection as the build-up of charge leads to a lesser packing density, while smaller conducting surface area causes beaded fibres (Bhardwaj & Kundu, 2010; Sousa Coelho et al., 2018). The collector can also be static or dynamic. Static collectors, classically aluminium foil, result in randomly arranged non-woven fibre meshes due to the bending instability of the jet. Dynamic collectors such as rotating drums, parallel electrodes, or mandrels obtain aligned parallel fibres. Fibre diameter was found to be decreased, while fibre structure was found to change from amorphous to more crystalline with increasing rotating speed. Furthermore, Young's modulus and tensile strength of fibres increased with increasing rotating speed up to point, after which they began to decrease (Kim et al., 2004; Sousa Coelho et al., 2018).

c) distance from tip to collector: there should be optimum time for the solvent to evaporate prior to collection, with 15 cm often being referenced in the literature. Too close can result in fused fibre webs, whereas too far a distance can result in fibre defects such as beads. Given those extremes, fibre morphology tends to progress from flatter with greater diameter to rounder and thinner as distance is increased (Bhardwaj & Kundu, 2010; Matabola & Moutloali, 2013; Sousa Coelho et al., 2018).

d) flow rate of solution: a minimum flow rate is needed in electrospinning to maintain an equilibrium Taylor cone. Yuan et al. (2004) found that for polysulfone/dimethylacetamide systems, bead defects were present at flow rates of 0.66 $ml.hr^{-1}$, whereas smooth, ultrafine fibres were formed at a flow rate of 0.40 $ml.hr^{-1}$. Zong et al. (2002) found similar while electrospinning of PLA solutions, with smaller fibres with spindle-like beads being produced at flow rates of 1.2 $ml.hr^{-1}$, while larger fibres with larger rounder beads were produced at rates of 4.5 $ml.hr^{-1}$. A lower flow rate limits bead formation by restricting the size of the droplet at the needle tip and allowing sufficient time for evaporation of the solvent. Too high a flow rate can result in fused webs as insufficient drying of the fibre occurs (Sousa Coelho et al., 2018).

e) diameter of the needle: He et al. (2019) found that while electrospinning polyethylene-oxide, that the obtained fibre diameter (assessed using scanning electron microscopy (SEM)) increased with needle diameter. They investigated the relationship between viscosity and shear rate of the polymer solution in the needle, using a plate-plate rheometer and a shear flow model, and concluded that at a constant flow rate, the viscosity of the polymer solution decreases as needle diameter decreases due to a greater

shear rate (which stretches the molecular chains out, allowing them to slide past one another more easily). For example, at a constant flow rate, they reported that as needle diameter was increased from 0.63 to 0.73 mm, shear rate decreased from 11.316 to 7.273 s^{-1} and viscosity increased from 2.41 to 2.54 Pa.s, with the resultant fibre diameter increasing from 179.9 to 219.8 mm. Increasing viscosity is related to larger diameter fibres as is discussed below.

f) ambient air humidity: in high humidity, water can condense on the fibres disrupting its morphology. Bae et al. (2013) found that while electrospinning polymethyl methacrylate polymer solutions, humidity of < 25% did not significantly impact fibre morphology however as humidity increased from 25% to 70%, the fibres became increasingly porous while maintaining their average diameter. Casper et al. (2004) also found that smooth, pore-free fibres were obtained when electrospinning polystyrene in tetrahydrofuran at 25% humidity, however pore number, diameter, size distribution and coalescence increased with humidity levels from 30% upwards. Conversely, at low humidity, evaporation of the organic solvent is expedited, and this can result in premature solidification of the fibre or needle tip clogging (Bhardwaj & Kundu, 2010).

g) temperature: Mit-uppatham et al. (2004) found that while electrospinning polyamide-6 solutions at different temperatures, the fibre morphology remained more or less the same except that the average fibre diameter decreased from 98 nm at 30 °C to 90 nm at 60 °C. The authors suggested that with increasing temperature there is expansion of the polymer molecules and less entanglement with overall reduction in viscosity; thus, there is less

opposition to stretching induced by the electric field. Additionally, there is increased evaporation of the solvent with rising temperature, and with excessively high temperatures, bio-active molecules which are incorporated into the fibre can become denatured (Sousa Coelho et al., 2018).

h) concentration of polymer solution: Matabola and Moutloali (2013) varied the concentration of polyvinylidene fluoride dissolved in N,N-dimethyl acetamide, and found the following: i) at < 17 wt% only beads were produced; ii) 17–22 wt% yielded a combination of beads and fibres; iii) 22–28 wt% yielded progressively smoother fibres with fewer bead-defects and increasing diameter; and iv) at ≥ 29 wt% the high viscosity of the solution made fibre production difficult. At lower concentrations, the polymer molecules are too dispersed to entangle to form fibres and in turn coil, aiding in the formation of droplets by the already high surface tension present in the low viscosity solution. At higher concentrations, there is sufficient polymer to entangle form fibres, and as concentration increase the rising viscosity limits the ability of the jet to elongate the fibres resulting in larger diameters. There exists a minimum concentration below which fibre formation is not possible, and a maximum concentration above which the viscosity restricts the flow of solution to the needle (Bhardwaj & Kundu, 2010; Matabola & Moutloali, 2013).

i) viscosity of electrospinning solution: this is influenced by concentration as well as ambient parameters like temperature. At low viscosities of < 1 poise, surface tension is the dominant factor in fibre morphology resulting in no continuous fibre formation and beads are produced. At high viscosities of > 20 poise there is difficulty maintaining flow of polymer solution to the

needle tip with possible clogging, and there is restriction to ejection of jets due to the high cohesive nature of the solution. Evidently, different polymers with differing molecular weights, have different inherent viscosities and unique optimum viscosity ranges in solution. The viscoelastic force tends to resist rapid changes in shape, and generally smoother fibres of larger diameter are produced with increasing viscosity within the optimum range (Bhardwaj & Kundu, 2010; Deitzel, Kleinmeyer, Harris, et al., 2001; Fong et al., 1999).

j) surface tension of electrospinning solution: this is usually a factor related to the solvent and aims to reduce the surface area per unit mass. A higher surface tension tends to induce instability in the jet and pull it into a bead formation (Bhardwaj & Kundu, 2010; Fong et al., 1999).

k) conductivity/surface charge density: conductivity is influenced by the polymer, solvent, and additional ionisable salts. Increased electrical conductivity correlates to a higher surface charge density of the electrospinning jet, and thus a higher net charge transported by the jet. This results in increased repulsive Coulombic forces within jet segments and thus increased stretching and elongation of the jet under the influence of the electric field, manifesting as more uniform fibres of smaller diameter with less bead-defects. The forces from increased surface charge density also try to increase surface area which resists bead formation. In two separate studies, addition of sodium chloride to polyethylene oxide solutions and polyvinylidene fluoride solutions both resulted in more uniform, smaller diameter fibres (Bhardwaj & Kundu, 2010; Fong et al., 1999; Matabola & Moutloali, 2013).

2.8 Electrospinning techniques

The parameters described above concern standard laboratory-based electrospinning, however the techniques and configurations involved can be altered greatly as the aims of electrospinning move from laboratory-based research to industrial and commercial high-throughput goals. The following are some examples of different set-ups of electrospinning:

a) multi-needle electrospinning: productivity is improved by increasing the number of jets emitted per unit time. However, the repulsive forces between the multiple jets (in addition to the effect of the electric field and the repulsive Coulombic forces within individual jets) leads to profound jet instability and difficulty maintaining uniform fibre morphology. Several parameters must be considered when utilising multiple needles: i) the spacing between needles which lessens repulsion between jets as it is increased but concentrates fibre deposition when it is decreased (though it should not be small enough to allow fusing of droplets at the needle tips); ii) the number and geometrical arrangement of the needles which should aim to maintain a constant electric field across all needles to ensure jet initiation occurs; iii) the lengths of individual needles with shorter lengths at the periphery helping to maintain uniform fibres; and iv) the flow rate which can be maintained as same across all needles by varying the internal diameter of the needles from the centre to periphery of the arrangement (Migliaresi, 2012; Xue et al., 2019).

b) needle-less electrospinning: this aims to overcome clogging that occurs with needle use. Porous tubes or flat electrodes with holes, through which the polymer solution is forced, can be utilised however are still prone to clogging. The game changed with the discovery that electrospinning jets can be emitted from the free surface of a liquid once there is a sufficient disturbance to cause accumulation of charge at a nidus enough to overcome surface tension. There are several different methods to concentrate the electric field and form this nidus such as floating the polymer solution on a ferromagnetic liquid and inducing spikes by a magnetic field, dripping polymer solution on a tilted metal edge, solid metal spinnerets/pins, and rotating discs (Migliaresi, 2012; Xue et al., 2019). One of the best examples of needle-less electrospinning used for commercial production is the patented SNC BEST™ ball-electrospinning technique employed by the Stellenbosch Nanofiber Company (2017), South Africa. It involves floating a rotating ball in a polymer solution so that it becomes thinly coated, and then subjecting the solution to a high voltage such that multiple jets eject from the free-surface as shown in Figure 6 (Kriel, 2015). Some of the issues highlighted with needle-less electrospinning techniques though are the wide variance in diameter and morphology of fibres obtained due to difficulty controlling jet uniformity, and the exposure of the free-surface of the polymer solution leading to evaporation or even ignition if corona discharge occurs (Migliaresi, 2012; Xue et al., 2019).



Figure 6: SNC BEST™ patented ball-electrospinning technology (still from a video taken from Stellenbosch Nanofiber Company (2017)).

c) manipulation of the electric field: fibre deposition can be made more precise over a smaller surface area by use of auxiliary electrodes (e.g., circular wires or tubes) around the spinneret or along the path of the jet. These electrodes usually have the same charge as the needle and cause convergence and concentration of the electric field lines along the spinning axis, thus reducing bending instabilities and controlling the widening, spiralling electrospinning jet (Figure 7A). Insulating tubes have also been used, as positive static charge accumulates on the inside surface of the tube. Nevertheless, intricate detail is not possible due to the nature of electrospinning. Alignment of fibres can be achieved through use of counter-electrodes as collectors. The negatively charged electrodes in formations such as parallel wires, or knife-edges act as electric field concentrators thus pulling the electrospinning jet towards them and generating a certain degree of alignment as a result (Figure 7B) (Sahay et al., 2011; Teo & Ramakrishna, 2006).

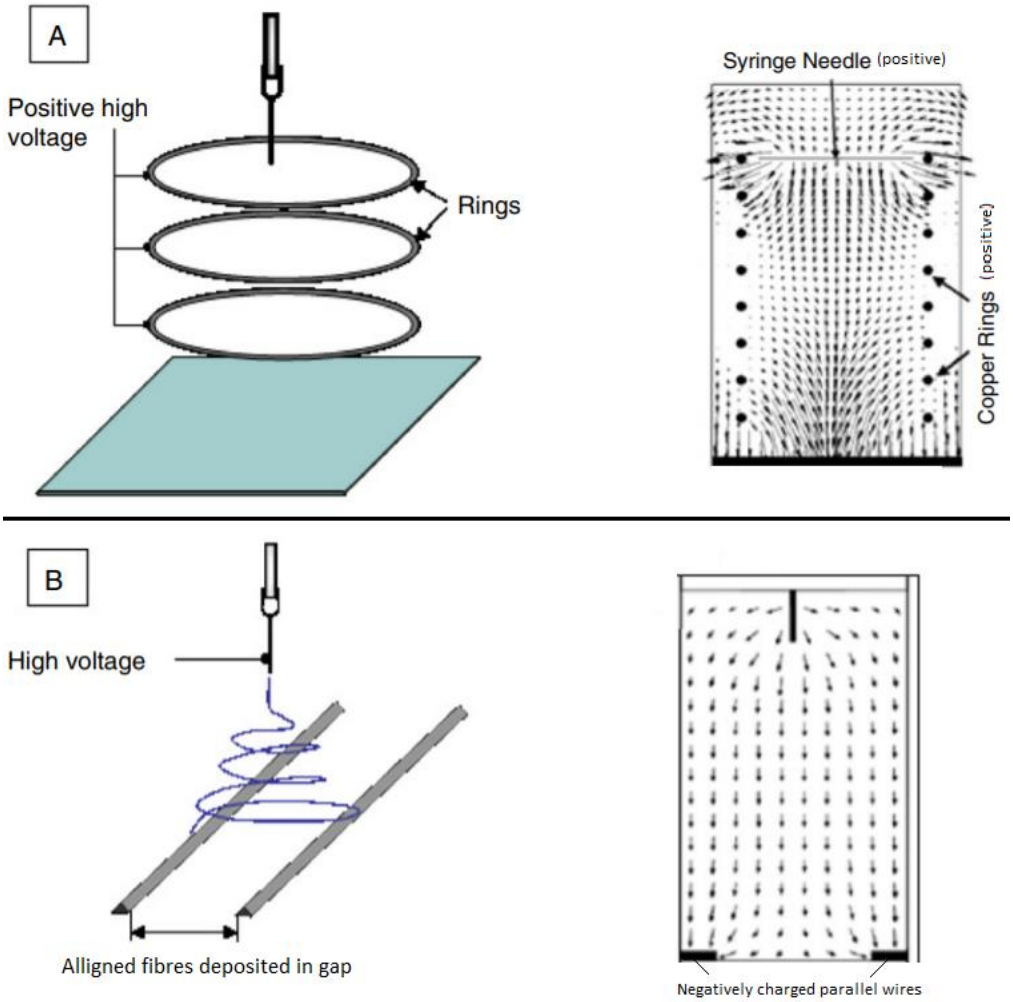


Figure 7: A: positively-charged wire rings as auxiliary electrodes to control fibre deposition with a diagram demonstrating convergence of electric field lines; B: negatively-charged parallel wire collectors to collect aligned fibres with a diagram demonstrating electric field lines concentrating into wires (adapted from Deitzel, Kleinmeyer, Hirvonen, et al. (2001); Li et al. (2003); Teo and Ramakrishna (2006)).

d) dynamic and liquid bath collectors: dynamic collectors as mentioned in section 2.7 are used to collect aligned fibres. Furthermore, electric field manipulation can be combined with dynamic collector set-ups to improve alignment or to collect aligned fibres over a smaller surface area (i.e., with

greater precision). For example, a knife-edge counter electrode positioned under a rotating collector can focus fibre deposition over the area of concentrated electric field, while the rotation results in fibre alignment. Cross-bar patterns can be produced using a sharp-pin electrode positioned inside a rotating cylinder which also has lateral movement; demonstrating the versatility that is possible with different configurations (Teo & Ramakrishna, 2006). Liquid deposition is another means of collection, with the liquid acting as a coagulation bath enhancing solidification of the electrospinning jet. Furthermore, fibres deposited on the liquid can be pulled into a continuous yarn of aligned fibres as it is dragged and elongated across the liquid's surface onto a rotating mandrel. Flowing water and even a water vortex can be used to collect continuous yarns. Liquids with high surface tension are preferred to prevent submersion of fibres into the bath, which can cause excess drag as it is pulled into a yarn (Migliaresi, 2012; Teo & Ramakrishna, 2006; Xue et al., 2019).

e) coaxial electrospinning: described in section 2.11.

2.9 Solvent choices for electrospinning

The solvent used is important to the electrospinning process and the eventual outcome of the fibres. Its first purpose is to dissolve the polymer in solution thus permitting electrospinning through jet formation. During dissolution, polymer-solvent interactions occur and can be either repulsive or attractive. Wannatong et al. (2004) while electrospinning polystyrene in different solvents found that as the solubility parameter of the solvent deviated from that of the polymer, the formation

of beads and bead diameter increased exponentially (r^2 parameter = 1.00). The differences in the solubility parameters results in the poor interaction between the polystyrene and solvent molecules with retraction of the polymer molecules to form beads. They found that even during preparation of the solutions, 3-methylphenol and N,N-dimethylformamide required mixing with polystyrene for a few days to form homogenous solutions, whereas tetrahydrofuran and toluene which had solubility parameters closer to polystyrene formed clear solutions after just six hours.

The solvent also carries the dissolved polymer molecules towards the collector, while undergoing evaporation and phase separation during jet thinning to allow formation of the final solid fibre (Bhardwaj & Kundu, 2010). Good volatility and a relatively lower boiling point facilitate evaporation during jet thinning, and Wannatong et al. (2004) found that of the different solvents used 3-methylphenol, which had highest boiling point at 203 °C, tended to produce wetter fibres with fused webs even when electrospun at 44 °C (as opposed to room temperature for the other solvents).

It has been mentioned previously that viscosity, surface tension, and solution conductivity affect fibre morphology. Veleirinho et al. (2008) electropsun polyethylene terephthalate in varying mixtures of trifluoroacetic acid and dichloromethane; and observed fibres of larger diameter with bead defects in mixtures with a higher dichloromethane ratio. Dichloromethane has a relatively lower dielectric constant which equates to solutions with lower conductivity and less stretching of the charged jet. Dichloromethane also has a relatively higher

surface tension which resists increasing surface area, and so contributes to formation of larger fibres (Veleirinho et al., 2008). Yang et al. (2004) also noted that a solution of ethanol with polyvinyl pyrrolidone produced smooth fibres of average diameter 250 nm, as compared to beaded fibres produced using solvents with higher surface tensions and lower viscosities, namely N,N-dimethylformamide and dichloromethane. Interestingly, when a 50/50 (w/w) mixture of N,N-dimethylformamide and ethanol was used, uniform bead-less nanofibers with diameters as low as 20 nm were obtained. It is suggested that the high dielectric constant and dipole moment of N,N-dimethylformamide is the instrumental factor by dissociating positive and negative charges through its electrolytic behaviour, facilitating dissolution of the polymer which develop positive ions on its chains in solution, and by raising the charge density of the solution (Yang et al., 2004).

Chloroform is a clear, colourless, liquid derivative of trichloromethane. It is volatile and has a characteristic pleasant, etheric odour. Chloroform has historically been used as an inhaled anaesthetic agent however, its use nowadays is limited to industry due to its toxicity. Chloroform has a boiling point of 62 °C, and at 20 °C is has a dielectric constant of 4.9, a surface tension of 27.1 $mN.m^{-1}$, and a viscosity of 5.63 millipoises (National Center for Biotechnology Information, 2022). Chloroform has been used extensively in electrospinning as a solvent, including dissolution of PLA to produce smooth fibres (Sawawi et al., 2017; Xu et al., 2017; Ye et al., 2019).

2.10 Polymer choices for electrospinning

To date there are hundreds of polymers that have used in electrospinning, and can be classified in terms of their origin, as either natural or synthetic.

Synthetic polymers have better mechanical properties such as viscoelasticity and strength, thermal stability, spinnability, and are more easily tailored to suit a desired purpose. They can be further sub-classified as either bio-based or fossil fuel-derived. The fossil fuel industry's contribution to global warming and pollution is being increasingly recognised, and that coupled with petroleum and natural gas being non-renewable resources, underlie intentions for the gradual phasing out of fossil-fuel derived polymers. Nevertheless, there remain numerous fossil-fuel derived polymers in widespread use such as polyvinyl alcohol (PVA) and poly-ε-caprolactone. Synthetic bio-based polymers are derived from renewable biological sources such as agricultural products (e.g., corn, potato, or soybeans), micro-organisms, algae, or crustaceans. Some examples include polylactides, polyhydroxyalkanoates, polyamides, and cellulose acetate. Regardless of whether they are fossil fuel-derived or bio-based, synthetic polymers can be biocompatible and biodegradable (or not), and those in commercial use are generally non-toxic. Furthermore, they can be broadly categorised as either hydrophobic or hydrophilic. Hydrophilic polymers have shorter degradation times and demonstrate faster burst release characteristics if functionalised. Hydrophobic polymers can be blended with hydrophilic polymers to control the release profiles of the fibres (Bhardwaj & Kundu, 2010; Gizaw et al., 2018; Liu et al., 2021; Soares et al., 2018).

Natural polymers are biological macromolecules found in nature and include proteins (e.g., collagen, gelatin, and hyaluronic acid, and silk fibroin),

polysaccharides (e.g., starch, cellulose, alginate, and chitosan), terpenes (e.g., natural rubber), and lipids. They originate from renewable sources, and can be water-soluble (e.g., alginates) or water-insoluble (e.g., chitosan). They are very biodegradable and are largely non-toxic and biocompatible. Natural polymers have a similarity to ECM in having an inherent capacity for binding cells through specific protein sequences, such as arginine/glycine/aspartic acid. However, compared to their synthetic counterparts, natural polymers are weaker and more fragile, prone to partial degradation or denaturation in certain electrospinning solvents, and are more difficult to electrospin because of their complex molecular makeup. These limitations can be improved by blending natural polymers with a carrier synthetic polymer (Bhardwaj & Kundu, 2010; Gizaw et al., 2018; Soares et al., 2018).

Polylactic acid (PLA) is a natural aliphatic polyester produced from carbohydrate food groups such as cassava, corn, and sugar cane. PLA is biodegraded in vivo (with a median half-life of 30 weeks) through hydrolysis into non-toxic and readily metabolised lactic acid. PLA is FDA-approved and used in many commercially available products including sutures and implants. PLA is chemically inert and so blending with another polymer is usually a prerequisite for further functionalization. Forming a composite material will also assist in cellular adhesion and integration. PLA has sufficient mechanical properties to form fibres through electrospinning and be used for wound dressings. It is soluble in several organic liquids (such as chloroform, dioxane, acetonitrile, and 1,1,2-trichloroethane) but not water, alcohol, and linear hydrocarbons; and this can complicate its use (Casalini et al., 2019; da Silva et al., 2018; Gómez-Pachón et al., 2014; Kanmaz et al., 2018).

Alginates are a group of naturally occurring anionic polymers obtained from brown seaweed of which Sargassum seaweed (which is found in Trinidad and Tobago) is a genus. Alginates are copolymers comprising of blocks of 1,4-linked β-D-mannuronate (M) and α-L-guluronate (G) residues. The blocks can be uninterrupted sequences of M or G, or sequences of alternating M and G; the length of blocks and the M:G ratio determines the type of alginate. The biocompatibility or rarely the immunogenicity of alginates can vary; higher purity alginates are less likely to illicit an immune response, the M:G ratio is important though not fully understood (intermediate G-content seems more biocompatible), and a higher viscosity also seems to improve biocompatibility. Alginates are FDA-approved and used in wound therapy as mentioned in section 2.5. The StayGuard™ Alginate Dressing by AdvaCare Pharma (2022) is an example of such a dressing. Alginates are also used in pharmaceuticals for controlled drug and protein release. Mammals lack the enzyme to degrade alginates, and the waste products of dissolution are not optimal for excretion (though in wound dressings, fluid containing dissolved products are lost directly to the external environment). However, certain steps such as oxidisation and having a greater percentage of low molecular weight alginates (though this compromises mechanical robustness) can improve degradation (Lee & Mooney, 2012; Tam et al., 2011). Electrospinning of alginates is difficult due to the repulsive forces among the polyanions, however blending alginates with another polymer can reduce these interactions and improve electrospinning; aside from loading the alginates with the desired bioactive agent (Bonino et al., 2011; Kyzioł et al., 2017).

PLA-alginate three-dimensional amalgams have been used as scaffolds for cellular attachment in osteochondral defects in canine femoral heads, and demonstrated a reparative response to immature cartilage at 6 weeks (Wayne et al., 2005). In vitro, PLA-alginate amalgam permitted cartilage differentiation with minimal fibrous deposition when seeded with marrow stroma-derived cells. It was rationalised that PLA provides mechanical stability for regenerating tissue that can biodegrade later on, whilst the alginate facilitates cell adhesion and retention with only minimal inflammatory reaction (Caterson et al., 2002).

2.11 Functionalization of electrospun fibres and different fibre morphologies

Electrospun micro/nano-fibrous scaffolds have large surface area-to-volume ratios, which lend themselves to being functionalised with drugs and other bioactive agents. Figure 8 shows some of the various techniques that can be employed to fabricate functionalised electrospun fibres:

a) physical adsorption: scaffolds are immersed in a liquid bath containing the desired agent, which then adsorbs onto the fibres through electrostatic interaction. While relatively easy to undertake, the release profile is uncontrollable (Feng et al., 2019). Nie et al. (2009) incorporated bone morphogenetic protein-2 plasmids onto polylactic-co-glycolic acid scaffolds as naked DNA coated onto the fibre surface, and as DNA-chitosan nanoparticles adsorbed onto the surface and incorporated within the electrospun fibres. These latter fibres demonstrated prolonged plasmid release beyond four weeks, however the burst release profile of the other two scaffolds actually helped accelerate the early phases of bone healing

within the first two weeks of use, in rodent in vivo experiments. Thus, while sustained release is desirable, release profile should be tailored to clinical need.

b) blend electrospinning: the agent is dissolved or dispersed within the polymer solution and becomes encapsulated within the fibre during one-phase electrospinning. However, organic solvents used to dissolve the polymer, as well as mechanical stirring used to make the blends homogeneous, can damage biomolecules and reduce their bioactivity. Agents encapsulated near the surface of the fibre still tend to undergo burst release within the first 24 hours, after which sustained release is maintained (Feng et al., 2019; Mohammadian & Eatemadi, 2017). Yang et al. (2014) electrospun ampicillin-loaded agar-polyacrylonitrile composite nanofibers and compared their release profile to ampicillin-loaded polyacrylonitrile nanofibers. The latter fibres released approximately 40% of its ampicillin load within 24 hours, and the remaining at a slower rate over the following five days. The ampicillin-loaded agar-polyacrylonitrile composite fibres had an initial fast release of 13% ampicillin in 24 hours followed by sustained release phase which reached 70% by seven days. The agar (within which the ampicillin was dissolved) was encapsulated within the polyacrylonitrile fibres, and this encapsulation phenomenon contributed to the sustained release. Dissolving the ampicillin directly in the polyacrylonitrile solution produced a fast matrix-type drug release.

c) emulsion electrospinning: this is an extension of blend electrospinning, in which the drug-containing hydrophilic water-phase is blended with a polymer-containing hydrophobic oil-phase, usually with use of a surfactant.

The need for a common solvent is eliminated, and so the desired biomolecule or drug can be combined with the most suitable polymer in their respective solvents. Furthermore, drug contact with the organic solvent is lessened, though the need for stirring or ultrasonication to obtain homogeneous emulsions can break up the water-phase droplets and expose the contents to the organic-phase, predisposing to damage to the bioactive agent (Mohammadian & Eatemadi, 2017).

Ye et al. (2019) performed water-in-oil emulsion electrospinning of sodium alginate (SA) solution in a PLA/chloroform organic phase using Span80 (sorbitane monooleate) surfactant. They obtained smooth, uniform, non-woven fibre meshes having fibre diameters of 250±90 nm. They also transformed the PLA-SA scaffolds into insoluble PLA-calcium alginate (CA) via ion exchange of Na^{+} with Ca^{2+} through immersion or spraying of the scaffold with calcium chloride ($CaCl_2$) solution. The PLA-CA fibres had 5-fold better elastic modulus and tensile strength in comparison to neat PLA fibres. Furthermore, percentage elongation at break of PLA-CA was as high as 110.8±10.9 % in comparison to 31.2±4.7 % for PLA fibres. Besides the improved mechanical properties, combining PLA with CA also improved the water absorption capacity (by almost 2-fold, p-value < 0.05) and improved the hydrophilicity of the scaffold (with a decrease in the water contact angle by approximately 6.5-fold, p-value < 0.05).

Xu et al. (2017) also performed emulsion electrospinning to obtain PLA-CA fibrous scaffolds. Interestingly, they found that SA:PLA weight ratios ranging

from 2.5–10 did not impact the morphology of the fibres, all having diameters of 250±90 nm. As the percentage of SA increased in the emulsion, so did the viscosity and the surface tension, and it is possible that these two factors balanced each other. The surfactant normally lowers surface tension, but as the amount of Span80 used was held constant, as percentage of SA increased so did the number of water-phase micelles and thus surface tension. It was also suggested that SA (and Span80) migrate to the surface of the nanofiber during electrospinning, based on findings of Fourier-transform infrared spectroscopy before and after soaking of the fibres in water. Xu et al. (2017) findings on mechanical properties, and hydrophilicity agreed with those made by Ye et al. (2019).

Ye et al. (2019) observed through SEM, the seeding of bone marrow stromal cells onto the surface of neat PLA and PLA-CA scaffolds. Cells were noted to have spread over the scaffold with pseudopodia while retaining their uniform morphology, indicating good adhesion and cellular activity. Both Ye et al. (2019) and Xu et al. (2017) utilised the MTT test with subsequent measurement of absorbance of the converted dye to assess proliferation of cells seeded onto scaffolds immersed in PBS. In both studies, PLA-CA scaffolds showed higher cellular proliferation than neat PLA scaffolds and control-culture plates, within the first five days of being seeded (after which insufficient space became the limiting factor to growth).

d) coaxial electrospinning: a coaxial needle, comprising of inner and outer concentric hollow needles, is used to obtain core-shell fibres. Two different fluids are driven at their individual flow rates through the separate needles,

combining at the tip to generate a compound Taylor cone. The inner and outer fluids should be viscous enough to maintain continuous jets, should be sufficiently immiscible in each other to maintain core-shell morphology during stretching, and should have similar dielectric properties to ensure they are acted upon equally by the electric field. Core-shell fibres can be utilised for sustained release by functionalising the inner polymer and optimising the thickness and degradation of the outer diffusive-barrier polymer (Chou et al., 2015; Xue et al., 2019).

Wang et al. (2010) electrospun different core-shell formations of both hydrophobic PLA and poly-3-hydroxy butyrate (PHB) with dimethyloxalylglycine drug. They found that for a drug-loaded PHB-core, and PLA-shell the release profile was burst or one-stage, achieving 70% cumulative release by about ≤ 10 days. On the other hand, drug-loaded PLA cores, with PHB-shells had two stage release: i) an initial burst release of 25% within the first 60 hours irrespective of shell thickness; and ii) a sustained linear release up to 70% by 12 days and 30 days for shell thicknesses of 120 nm and 230 nm respectively. Afshar et al. (2019) electrospun curcumin drug-functionalised PLA-chitosan core-shell fibres (diameters 671±172 nm) and found: i) when curcumin was incorporated into the chitosan-shell a burst release of 80% within the first 10 hours was reached due to the degradation of chitosan in aqueous solution; and ii) when incorporated into the PLA-core, release was 25% within the first four hours (due to diffusion of curcumin into the shell) and then sustained release to 80% by 120 hours. Interestingly, it was a combination of a hydrophobic core

with an easily degradable shell (as opposed to a barrier-shell) that provided the sustained release characteristics.

e) surface modification: this involves covalent immobilization of agents on the electrospun fibre surface. This can make the scaffolds similar to natural tissues thus improving incorporation in vivo. Miroshnichenko et al. (2019) plasma-coated polycaprolactone electrospun nanofibers with a COOH layer, and then immobilised platelet-rich plasma proteins on the surface through covalent binding of their NH_2-groups with the COOH-groups. They found reduced human fibroblast cell apoptosis and an increased cell proliferation in vitro, when compared to scaffolds comprised of neat polycaprolactone, polycaprolactone with plasma-coated COOH, and polycaprolactone with non-covalently bonded platelet-rich plasma proteins. While covalent immobilisation can be used to limit burst release, it poses an issue for agents that must be internalised by cells as they a fixed to the fibres' surface. Local external factors and enzymes can be employed to regulate the release of the agent in these cases.

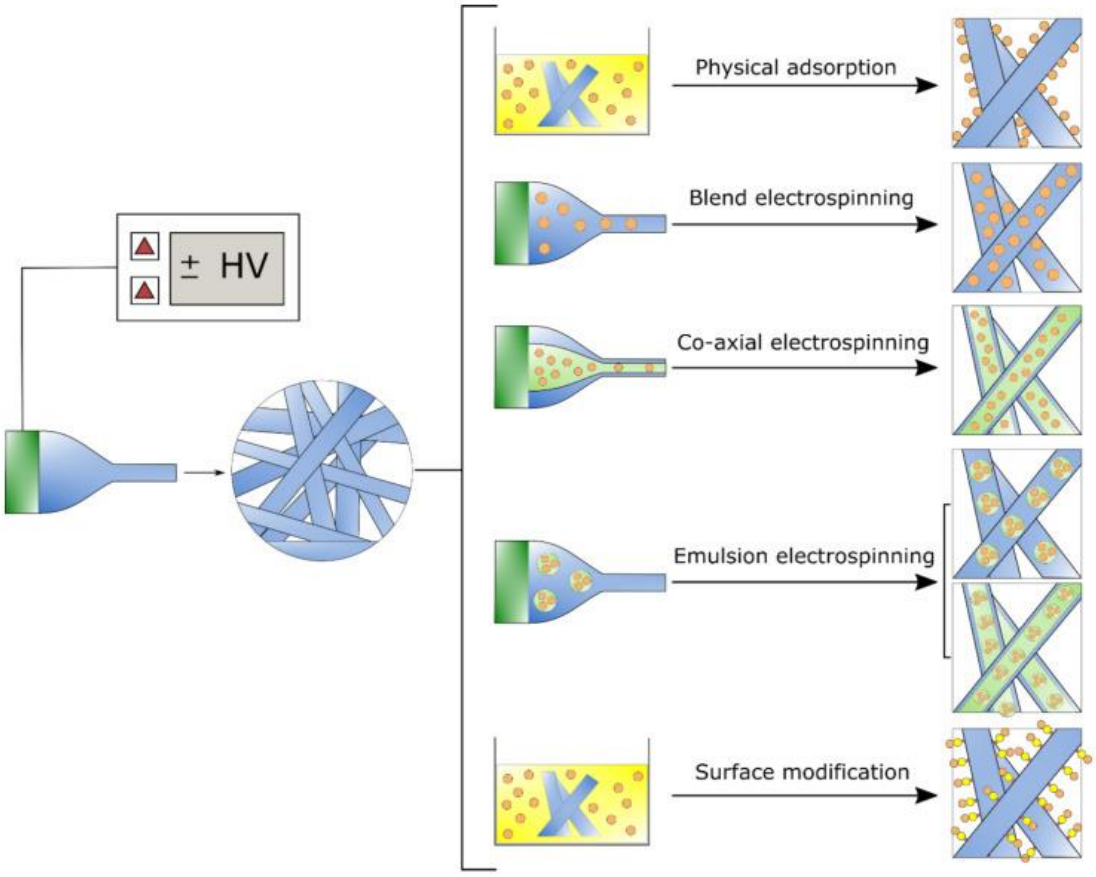


Figure 8: Fabrication techniques for functionalised electrospun fibres (taken from Azimi et al. (2020)).

Although the classic smooth, cylindrical electrospun fibre is the most referenced, there exist several other fibre morphologies due to the versatility of electrospinning:

a) core-shell fibres: these have been discussed above in this section. Kharaghani et al. (2019) demonstrated the ability of core-shell fibres to deliver both water-soluble and organic-phase drugs. They immersed diclofenac sodium loaded-PVA core nanofibers in polyacrylonitrile-gentamicin sulphate to form the core-shell structure, and then confirmed and characterised the release of both drugs in vitro.

b) bead-on-string fibres: previously thought to be a useless by-product, these fibres may pose useful in controlling drug release, thus allowing the release profile of crucial agents to be synchronised to when raised levels are physiologically appropriate in wound healing. They can be produced by manipulating traditional electrospinning (where previously parameters had to be optimised to avoid bead defects, as seen in section 2.7), coaxial electrospinning, and by emulsion electrospinning (Zhao & Chi, 2018). Qi et al. (2006) performed water-in-oil emulsion electrospinning of bead-on-string CA-microspheres in an organic continuous phase of PLA, using an AOT surfactant (sodium bis-2-ethylhexyl sulfosuccinate). They cross-linked the alginate in the emulsion into CA with $CaCl_2$ prior to electrospinning, thus producing the CA-microspheres. This method is depicted most clearly in Figure 9. To functionalise the scaffolds with bovine serum albumin (BSA), they incorporated it into the alginate solution prior to emulsification. When these emulsions were electrospun at 15 kV, round 'beads' with relatively large diameter 'strings' were obtained, which stretched out into narrower diameter 'strings' and spindle-shaped 'beads' at 20 kV. Release profiles of BSA from the bead-on-string fibres had an initial burst release followed by a sustained release achieving about 80% cumulative release by 60 hours, as compared to a burst release of about 90% within ten hours for naked CA-microspheres. Intriguingly, the spindle-shaped fibres always had higher cumulative release profiles within the first 50 hours, likely due to the spindle-shape causing the CA-microspheres to be closer to the fibres' surface.

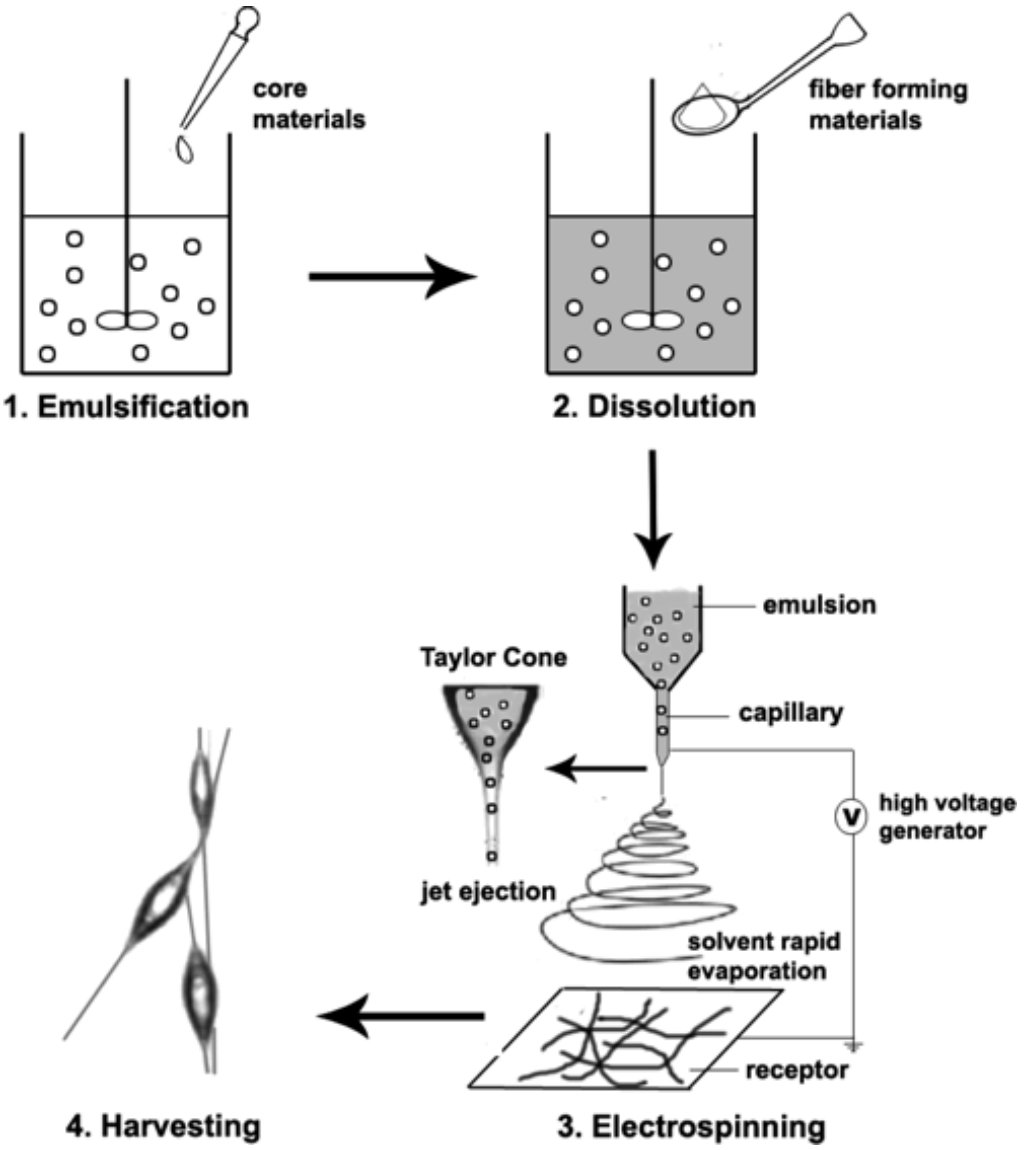


Figure 9: Overview of the major steps of microencapsulation in fibres by emulsion electrospinning as done by Qi et al. (2006).

Li et al. (2017) electrospun polylactic-co-glycolic acid in a mixed solvent of chloroform and acetone, and varied the bead diameters by adjusting the ratio of solvents and concentration of polymer. They functionalised the various scaffolds with tetracycline hydrochloride and found that larger diameter beads of 2.45 μm had significantly (p-value ≤ 0.05) more sustained

release than beads of 0.93 μm in size with release rates of 11.2 % and 27.9% at 30 minutes, and 79.0% and 89.3% at 48 hours respectively.

c) porous fibres: this refers to pores on the electrospun fibre itself, rather than the gaps between the individual fibres in a scaffold. Porous fibres increase the overall surface area-to-volume ratio of the scaffold, which facilitates increased cellular attachment and interaction, and increased protein adsorption. They can result in a significant burst release of loaded drugs where this is desirable, such as an initial burst release of antibiotics to limit microbial proliferation. Porosity can be achieved through various phase separation mechanisms and selective removal. The breath figures mechanism is the most encountered and has been previously alluded to in section 2.7: in the presence of high humidity, the temperature drop that occurs with solvent evaporation results in condensation of water vapour droplets on the semi-dried electrospinning fibre, which eventually results in pores after complete evaporation of the solvent and water (Huang & Thomas, 2020).

d) other various fibres morphologies have been described such as ribbon-like, wrinkled-surface, and helical, though they have not been as extensively investigated (Migliaresi, 2012; Yang et al., 2004).

2.12 Papaya-incorporated electrospun scaffolds

There is an increasing interest in the use of plant-derived compounds to functionalise micro/nano-fibrous scaffolds. Plant compounds can be incorporated in the form of extracts, essential oils, or pure active ingredients. Obtaining the latter

two is complex, whereas obtaining plant extracts is relatively simple especially through the method of soaking or macerare (Figure 10). Water or organic solvents can be used to extract the active ingredient, alongside other dissolvable compounds, from fresh or dried plant products. Numerous herbal extracts have been previously incorporated into electrospun fibres including green tea, soursop, aloe vera, moringa, and turmeric (Fatehi & Abbasi, 2020); and papaya as is discussed below.

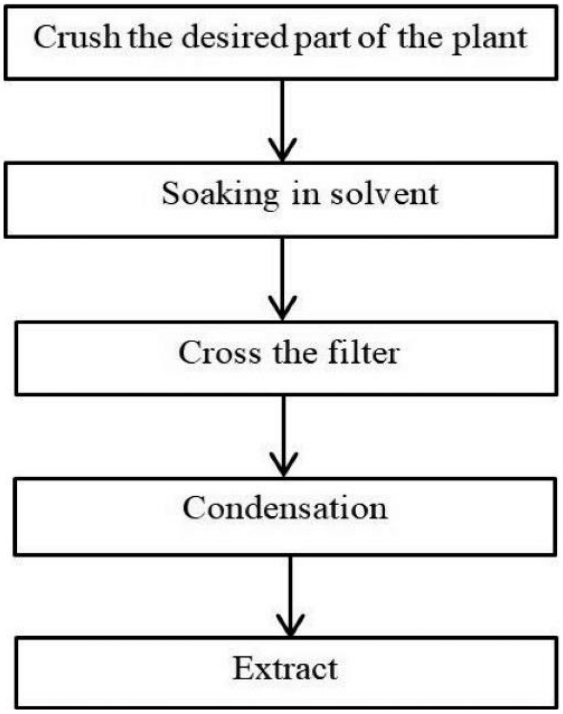


Figure 10: Basic steps in the soaking method to obtain a plant extract (taken from Fatehi and Abbasi (2020)).

Ahlawat et al. (2019) electrospun papaya leaf extract-loaded PVA-gelatin nanofibrous scaffolds. They extensively characterised the scaffolds, finding: i) uniform, smooth fibres with diameters of 140±20 nm; ii) an amorphous nature from X-ray diffraction analysis; iii) enhanced thermal stability as compared to neat PVA-

gelatin nanofibers; iv) a surface roughness of 286.707 nm based on atomic force microscopy; and v) a maintained hydrophilicity when compared to neat PVA-gelatin fibres having a water contact angle of 74.9°. Antibacterial activity in vitro was also demonstrated in a colony forming unit method and disc diffusion method, against a PVA-gelatin control. Haemocompatibility was confirmed through the platelet adhesion test with papaya-incorporated fibres adhering platelets less than the neat PVA-gelatin fibres. Additionally, absence of cytotoxicity to mouse embryonic fibroblast cells in vitro was demonstrated: i) via the MTT assay when compared to neat PVA-gelatin (with 80% cell viability after 24 hours for both); and ii) via morphological analysis of stained seeded cells when compared to the absence of nanofibers (with no significant differences in cell morphology). Ahlawat et al. (2019) incorporated the papaya leaf extract powder directly into the hydrophilic PVA-gelatin blend prior to electrospinning; and confirmed its presence in the nano-scaffold by characteristic peaks on infrared spectroscopy, and the presence of zinc, iron, magnesium, potassium, and aluminium metals on energy dispersive X-ray analysis (EDX). While the scaffolds produced by Ahlawat et al. (2019) are promising, PVA is fossil-fuel based while gelatin is derived from animal sources which has religious implications in Trinidad and Tobago; and so other natural sources as described above maybe more favourable for local production and use.

Hussain et al. (2017) produced papaya leaf extract-loaded CA fibres through extrusion of papaya extract incorporated-SA solution into a $CaCl_2$ bath. When compared to neat CA fibres, they found that the water absorption properties of the papaya-CA fibres decreased, but that the papaya conferred antibacterial properties in vitro by reducing S aureus growth by 85%. Balaji et al. (2016) electrospun

polyurethane nanofibrous scaffolds functionalised with a combination of papaya epicarp extract (using the same extraction method as used by Nayak et al. (2007)) and honey extract. They observed uniform, ribbon-like fibres with a mean diameter of 190±19.93 nm. Furthermore, they assessed percentage porosity through the density bottle method and found a 4% increase (due to increased fibrous density) when compared to neat polyurethane scaffolds. The mean pore size of the functionalised scaffold was 12.54±0.58 μm which falls just short of the optimum range of 20–120 μm needed for infiltration of skin cells (Elsner et al., 2012). The incorporation of papaya and honey improved the hydrophilicity of the polyurethane scaffolds by 13–14%, and increased water absorption 3-fold. Haemocompatibility was demonstrated by the functionalised scaffolds having a 45% better albumin binding, a 24% reduced clot-forming fibrinogen adsorption, longer activated partial thromboplastin and prothrombin times (tests for coagulation), and a 0.86% (versus 2.66%) haemolysis percentage when compared to neat polyurethane scaffolds (p-value < 0.05). This group though has not reported further testing or development of this technology in the intervening four years; and it is difficult to distinguish the properties of the scaffold that have been conferred by the papaya extract as opposed to the honey extract.

This section has served to emphasise the need for more effective wound care and identify electrospun scaffolds as a technology that may fulfil the requirements to provide such improved efficacy. Furthermore, the many advantages of using abundant, naturally derived papaya extracts in wound healing have been discussed. The case for the combination of nanofibrous dressings containing papaya extract

has therefore been made and the scene set for the work in the following sections which explores this possibility experimentally.

3. Research questions

The aims of this study were therefore:

a) To produce a neat CA-PLA micro/nanofibrous scaffold utilising emulsion electrospinning.
b) To incorporate Carica papaya L. extract into a CA-PLA micro/nanofibrous scaffold.
c) To obtain both smooth fibre and bead-on-string fibre morphologies in both (a) and (b).
d) To assess the gross and microscopic appearance of the obtained scaffolds.

4. Methods

4.1 Equipment

The AHVAC30KVR5MABT high-voltage power supply was purchased from Analog Technologies Inc, United States. The IPS-12 syringe pump was purchased from Inovenso Technology Inc, Turkey. All other equipment and glassware were standard in the laboratory.

4.2 Materials

Carica papaya L. unripe green fruits, and green healthy leaves were obtained locally from home-grown trees. Sodium alginate (SA) CAS-No 9005-38-3 (laboratory grade) was purchased from Henan Tianfu Chemical Co Ltd, China. Poly-L-lactic acid (PLA) CAS No 33135-50-1 (technical grade) was purchased from BOCSCI Inc, United States. Chloroform CAS No 67-66-3 (analytical grade) was supplied from VWR International SAS, France. Calcium chloride ($CaCl_2$) powder Product No 262244W (technical grade) was supplied from BDH Laboratory Supplies, England. Span60 (sorbitane monostearate) and 0.5 M sodium hydroxide solution were obtained from stores already present at the laboratory. Water was distilled as needed, but all other chemicals were used without further purification.

4.3 Obtaining the papaya extract

The papaya extract was obtained using a hybrid method based on Nayak et al. (2012); Nayak et al. (2007) and Asghar et al. (2016). Unripe green fruits and leaves of Carica papaya L. were washed with tap then distilled water and left to air dry. The fruits were scrubbed to remove the thin green layer and 500 g of epicarp was blended with 1250 mL distilled water. The dark brown seeds of the fruits were collected and washed with tap then distilled water and left to air dry. 150 g of seeds and 500 g of leaves were blended with 375 mL and 1250 mL of distilled water respectively. The mixtures were covered and left to sit for 72 hours, being shaken periodically. The mixtures were combined then filtered through a Gooch crucible and then grade one qualitative filter paper. The clear, orange-coloured filtrate was left to air evaporate while being warmed to 45 °C and stirred using a magnetic stirrer, until a final volume of 1150 mL was obtained. The resulting concentrated papaya-extract solution was filtered once more using a Millex® syringe filter with 5 μm pore size, before further use in these experiments.

4.4 Electrospinning apparatus

Electrospinning apparatus was set-up as shown in Figure 11 in a fume hood, and a protocol adapted from the Institute of Biomedical Engineering, University of Oxford was utilised. Electrospinning was conducted at atmospheric pressure and at an ambient temperature of 20 °C; however, all electrospinning solutions were warmed at a setting of 35 °C on a hot plate/magnetic stirrer while being stirred prior to electrospinning. A 3 mL-syringe with a 20-gauge (0.6 mm internal diameter) flat-end metal needle attached, positioned horizontally in the syringe pump, was utilised in all these electrospinning experiments. Also standard throughout was use

of an aluminium foil collector positioned 15 cm from the needle tip. The high-voltage DC power supplied was varied between 15–25 kV, and the syringe feed rate was adjusted between 0.3–0.5 mL.hr^{-1} depending on the solution being electrospun to optimize Taylor cone formation with jet initiation and minimize electrospraying.

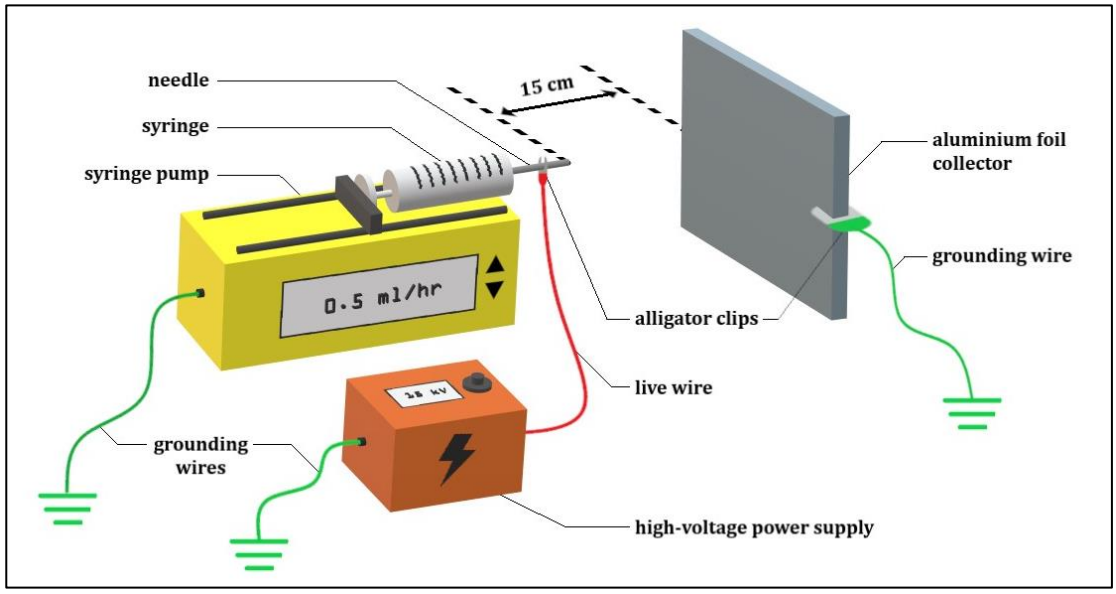


Figure 11: Electrospinning apparatus set-up.

4.5 Preparation of neat CA-PLA smooth fibre electrospun scaffolds

A method adapted from Xu et al. (2017) and Ye et al. (2019) was utilised. SA was dissolved in distilled water to obtain a 40 mg.mL^{-1} aqueous solution. 0.3 g of Span60 was dissolved in 10 mL chloroform, and then 3.6 mL of 40 mg.mL^{-1} SA solution was mixed into this while stirring at 1600 rpm using a magnetic stirrer for 30 minutes. Lastly, 1.92 g of PLA was added to this mixture and stirred at 600 rpm for six hours until a uniform emulsion was obtained. Emulsions were then electrospun at a voltage of 15 kV with a syringe feed rate of 0.5 mL.hr^{-1}. Scaffolds were then

immersed in a 10 mg.mL^{-1} aqueous $CaCl_2$ bath, and then left to air dry for 24 hours before further analysis.

4.6 Preparation of neat CA-PLA bead-on-string fibre electrospun scaffolds

A method adapted from Xu et al. (2017), Ye et al. (2019) and Qi et al. (2006) was utilised. SA was dissolved in distilled water to obtain a 40 mg.mL^{-1} aqueous solution. 0.3 g of Span60 was dissolved in 10 mL chloroform, and then 3.6 mL of 40 mg.mL^{-1} SA solution was mixed into this while stirring at 1600 rpm using a magnetic stirrer for 30 minutes. Then 1 mL of 50 mg.mL^{-1} $CaCl_2$ solution was added to the mixture while continuing to stir for a further 20 minutes. Finally, 1.92 g of PLA was added to this mixture and stirred at 600 rpm for six hours until a uniform emulsion was obtained. Emulsions were then electrospun at a voltage of 15 kV with a syringe feed rate of 0.5 mL.hr^{-1}. Scaffolds obtained were ready for further analysis.

4.7 Preparation of papaya-functionalised CA-PLA smooth fibre electrospun scaffolds (using $CaCl_2$)

This was prepared using the same method as described in section 4.5 except that SA was dissolved in equal volumes of papaya extract and distilled water, to make up the final concentration of 40 mg.mL^{-1} SA. Emulsions here required electrospinning at a voltage of 20 kV with a syringe feed rate of 0.3 mL.hr^{-1}.

4.8 Preparation of papaya-functionalised CA-PLA bead-on-string fibre electrospun scaffolds (using $CaCl_2$)

This was prepared using the same method as described in section 4.6 except that SA was dissolved in equal volumes of papaya extract and distilled water, to make up the final concentration of 40 $mg.mL^{-1}$ SA. Emulsions here required electrospinning at a voltage of 20 kV with a syringe feed rate of 0.3 $mL.hr^{-1}$.

4.9 Analysis of papaya extract for calcium

To 50 mL of papaya extract in a clear conical flask, 0.5 M sodium hydroxide solution was added dropwise and then in excess, looking for formation of a white precipitate that was insoluble in excess sodium hydroxide.

Ionized calcium in the papaya extract was tested for using a point-of-care biochemistry analyser (Stat Profile® pHOx® Ultra, Nova Biomedical), which utilises an ion-selective electrode methodology.

4.10 Preparation of papaya-functionalised CA-PLA electrospun scaffolds (without use of $CaCl_2$)

SA was dissolved in distilled water to obtain an 80 $mg.mL^{-1}$ aqueous solution. 0.3 g of Span60 was dissolved in 10 mL chloroform, and then 1.8 mL of 80 $mg.mL^{-1}$ SA solution was mixed into this while stirring at 1600 rpm using a magnetic stirrer for 30 minutes. Then, 1.92 g of PLA was added to this mixture and stirred at 600 rpm

for six hours until a uniform emulsion was obtained. Finally, 1.8 mL of papaya extract was added dropwise to this emulsion and stirred at 600 rpm for a further two hours until homogenous again. Emulsions were then electrospun at a voltage of 25 kV with a syringe feed rate of 0.5 $mL.hr^{-1}$. Scaffolds obtained were ready for further analysis.

4.11 Physical and morphological assessment of electrospun scaffolds

Gross physical appearance and integrity of the scaffold mats were assessed by visual inspection. Morphology of the electrospun fibres were assessed using bright-field, oil-immersion, 100× magnification optical microscopy, with use of an ocular micrometer. Angeles et al. (2008) utilised optical microscopy effectively to assess electrospun emulsion microfibers (of diameters ≤ 2 μm) and their morphology, namely the breakup of emulsion droplets to produce bead-on-string fibres.

5. Results and Discussion

5.1 Preparation of emulsions and electrospinning process

There were no observable differences in emulsions produced for generation of both neat CA-PLA smooth and bead-on-string fibres (as described in sections 4.5 and 4.6 respectively), both being homogeneous, milky white liquids with a relatively thick viscosity (similar to white glue). During electrospinning, both emulsions generated Taylor cones with fine electrospinning jets (not visible to the naked eye) and infrequent electrosprayed droplets. However, the emulsion designed to create bead-on-string fibres intermittently produced thicker electrospinning jets (barely visible as a thin fibre as seen in Figure 12) which 'whipped' onto the collector.

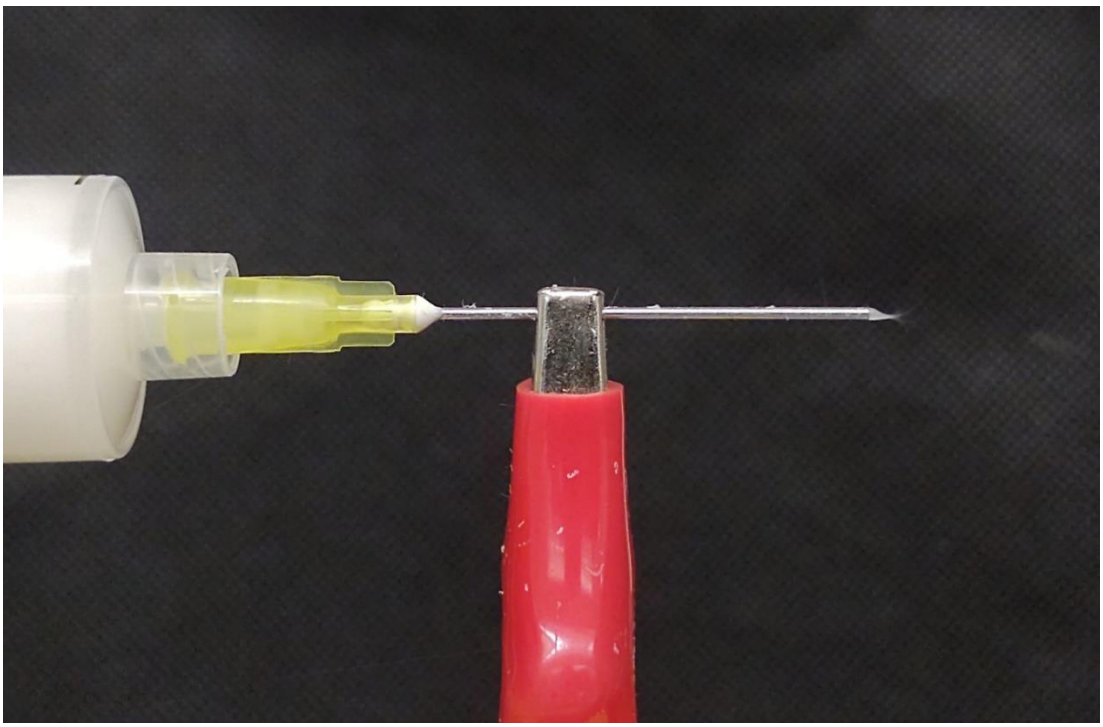


Figure 12: Electrospinning of neat CA-PLA bead-on-string emulsions. Visible are the flat-ended needle spinneret with attached high-voltage alligator clip, and the Taylor

cone with the just visible thin-fibre jet. The external diameter of the needle is 0.9 mm. Images were captured using the 48-megapixel 1.6 μm Quad Pixel camera on a Motorola One Fusion phone.

The emulsions for the papaya-functionalised CA-PLA smooth and bead-on-string fibres in which $CaCl_2$ was used (as described in sections 4.7 and 4.8 respectively), both appeared as inhomogeneous colloids with visible, firm, orange-coloured globules amongst a continuous phase of a relatively thick, opaque, cream-coloured liquid. The globules were approximately ≤ 1.0 mm in diameter, however the emulsion designed to produce bead-on-string fibres had more of the larger globules with more aggregation. During electrospinning, both emulsions generated bursts of electrospinning jets interrupted frequently by visible electrosprayed droplets. The electrospinning jets varied in thickness from being not visible to the naked eye, to being just visible as a thin fibre (similar to that seen in Figure 12); with the emulsion designed to produce bead-on-string fibres generating more of the thicker jets. The needle clogged often with the orange-coloured globules, and the syringe had to be periodically removed and purged.

Concerns were raised about the impact of raised calcium ion levels in papaya extract on premature CA formation with subsequent aggregation and needle clogging (explained further in section 5.2), hence tests were run without addition of $CaCl_2$. The emulsion designed to produce the papaya-functionalised CA-PLA scaffold without the use of $CaCl_2$ (as described in section 4.10), appeared as a homogeneous colloidal mixture with clear, orange-tinged submillimetre droplets dispersed amongst a continuous phase of the apricot-coloured, opaque liquid. It had

a less viscous consistency as compared to the previous emulsions which utilised $CaCl_2$. During electrospinning, Taylor cone formation with jets ranging from not visible to the naked eye to barely visible as a thin fibre were noted. The jets were not as continuous as the neat CA-PLA emulsions, breaking off into smaller strands. The jets were also disrupted intermittently by electrospraying of droplets, but not as frequently as the papaya-functionalised emulsions which utilised $CaCl_2$. Additionally, no clogging of the needle occurred. It is likely therefore that $CaCl_2$ omission and appropriate timing for addition of the papaya extract were important steps in improving the process.

5.2 Impact of papaya on alginate-PLA emulsion

Soluble sodium alginate (SA) can be converted to insoluble calcium alginate (CA) through use of calcium chloride ($CaCl_2$) solution in which the Ca^{2+} ion replaces the Na^{+} ion. Addition of $CaCl_2$ to the scaffold and formation of CA also results is cross linking of the fibres (Qi et al., 2006; Ye et al., 2019). The mineral composition of papaya is known to include significant amounts of calcium. Marfo et al. (1986) found that papaya seeds contained 17,340 $\mu g.g^{-1}$ of calcium (more than any other mineral) using wet-ash extraction and atomic absorption spectrophotometry. Nwofia et al. (2012) also found relatively high levels of calcium in the leaves (267.20–366.07 $mg.100g^{-1}$), seeds (45.43–54.44 $mg.100g^{-1}$), and fruit pulp (21.38–34.73 $mg.100g^{-1}$) across different papaya morphotypes, using dry-ash extraction and the versanate EDTA complexometric titration method.

It was suspected that the use of papaya extract to formulate the 40 $mg.mL^{-1}$ SA solution caused premature conversion to CA, which resulted in the globules in the inhomogeneous colloidal emulsions using this solution. These insoluble, firm, papaya-incorporated CA globules could not have been broken down by the magnetic stirrer to form uniform emulsions and were likely not included in the electrospinning jet (actually clogging the needle and having to be purged out). Figure 13 compares the 40 $mg.mL^{-1}$ SA solution using distilled water alone, to that which incorporated papaya extract. It is evident that the latter was more viscous and gelatinous, and less smooth, with firm clumps being noted.

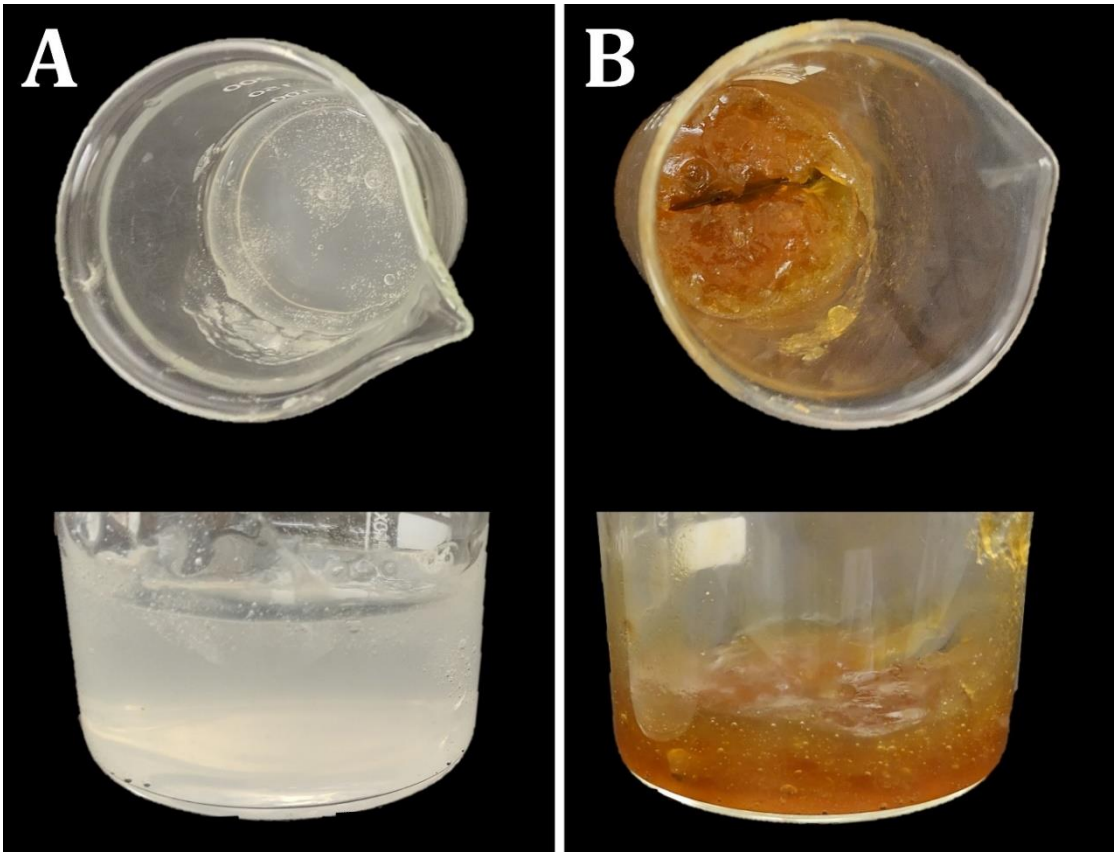


Figure 13: A: 40 $mg.mL^{-1}$ SA and distilled water solution; B: 40 $mg.mL^{-1}$ SA solution using equal parts distilled water and papaya extract, which was used in sections 4.7 and 4.8 of the methodology.

As such, testing to confirm the presence of calcium in the papaya extract was done. Qualitative testing using sodium hydroxide was unsuccessful. The cloudy fine white precipitate of calcium hydroxide which normally forms, was unable to be appreciated in the orange-coloured papaya extract. However, analysis using the point-of-care biochemical analyser yielded a concentration of ionised calcium of 1.16 $mmol.L^{-1}$ (or approximately 4.65 $mg.dL^{-1}$); thus, confirming the presence of calcium ions in the papaya extract used.

This analysis prompted the decision to forgo the use of $CaCl_2$ solution in making the scaffolds and recognise papaya extract as an appreciable source of Ca^{2+}. Thus, the method as described in section 4.10 was undertaken, with the intention to form a uniform water-in-oil emulsion of SA in PLA/chloroform first, and then add the papaya extract prior to electrospinning. The actual emulsion observed (as described in section 5.1) could be explained by the papaya extract being dissolved into the 'water' aspect of water-in-oil emulsion (i.e., the SA droplets) at the point that it is added, with the CA that is formed remaining as fine droplets, thus maintaining a uniform emulsion.

5.3 Gross appearance of electrospun scaffolds

Electrospinning was conducted for at least two hours for each emulsion, such that a thin membrane was obtained. The gross appearance of the electrospun scaffolds can be seen in Figure 14. All scaffolds were opaque white in colouration. Both neat CA-PLA scaffolds had the character of fine tissue paper. Upon visual comparison to

pictures published in their article, the neat PLA-CA membranes produced by Ye et al. (2019) had a thicker but otherwise similar appearance to the membranes obtained in this study. The scaffolds obtained in this experiment were able to be torn into strips (tearing like felt) and separated from the aluminium foil collector relatively easily while maintaining their integrity as a membrane. The neat CA-PLA emulsion designed to produce bead-on-string fibres had more wrinkles, likely a result of the intermittent thicker electrospinning jet.

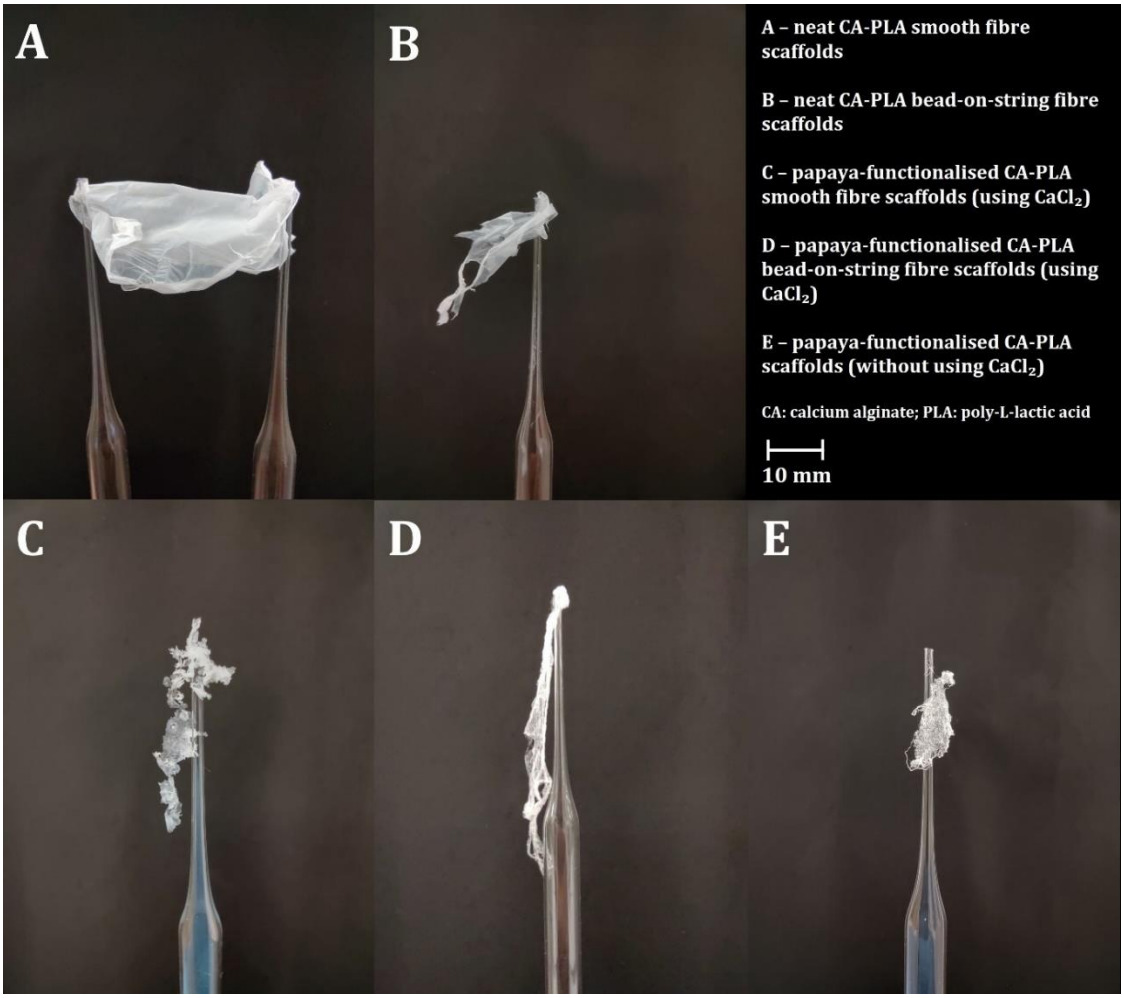


Figure 14: Gross appearance of electrospun scaffolds. Images were captured using the 48-megapixel 1.6 µm Quad Pixel camera on a Motorola One Fusion phone.

The membranes produced by the papaya-functionalised CA-PLA emulsions lacked the integrity of the neat CA-PLA scaffolds. The scaffold produced using the papaya-functionalised CA-PLA smooth fibre emulsion in which $CaCl_2$ was used, had a fragile, crystalline appearance like frost on a glass. It tore easily upon peeling from the foil collector, and while handling. Furthermore, it was non-uniform with thicker areas of the membrane likely resulting from electrospraying of droplets. The scaffold produced using the papaya-functionalised CA-PLA bead-on-string fibre emulsion in which $CaCl_2$ was also used, had the appearance of thick cobweb, which collapsed into a yarn upon peeling from the collector and tore easily. Finally, the scaffold produced from the papaya-functionalised CA-PLA emulsion in which $CaCl_2$ was not used, had the appearance of a fine jute felt. It peeled from the collector piecemeal, with individual patches separating easily from each other. Additionally, the individual patches resisted tearing better than the other papaya-functionalised scaffolds, however it still tore relatively easily in comparison to the neat CA-PLA scaffolds. Ahlawat et al. (2019) did not explicitly describe the gross appearance of their papaya extract-loaded PVA-gelatin nanofibrous scaffolds, nor provide any obvious pictures in their paper which could have been used for comparison. However, it must be acknowledged that they did not employ emulsion electrospinning, rather using a hydrophilic blend of synthetic and animal-derived natural polymers, in addition to a soluble papaya leaf-extract powder.

5.4 Microscopic morphology of electrospun scaffolds

The microscopic appearances of the electrospun scaffolds are shown in Figure 15. The scaffolds obtained using the neat CA-PLA emulsion designed to produce smooth

fibres, did in fact produce uniform smooth microfibers having diameters of ≤ 0.5 μm. These scaffolds most resembled those archetypal non-woven electrospun scaffolds described in the literature. Xu et al. (2017) and Ye et al. (2019) who both performed emulsion electrospinning of PLA-CA fibres both recorded diameters of 250±90 nm. This is nearly half the diameter of the fibres recorded in this experiment, however while an ocular micrometer, in which the smallest graduation represented 2 μm, was used in this experiment, both those authors employed an SEM thus delivering a more precise analysis. Interestingly, both those authors obtained fibre diameters of 780±200 nm for neat PLA in chloroform, and it is possible that some of the larger diameter fibres produced in this experiment were PLA fibres that may have escaped emulsification with SA.

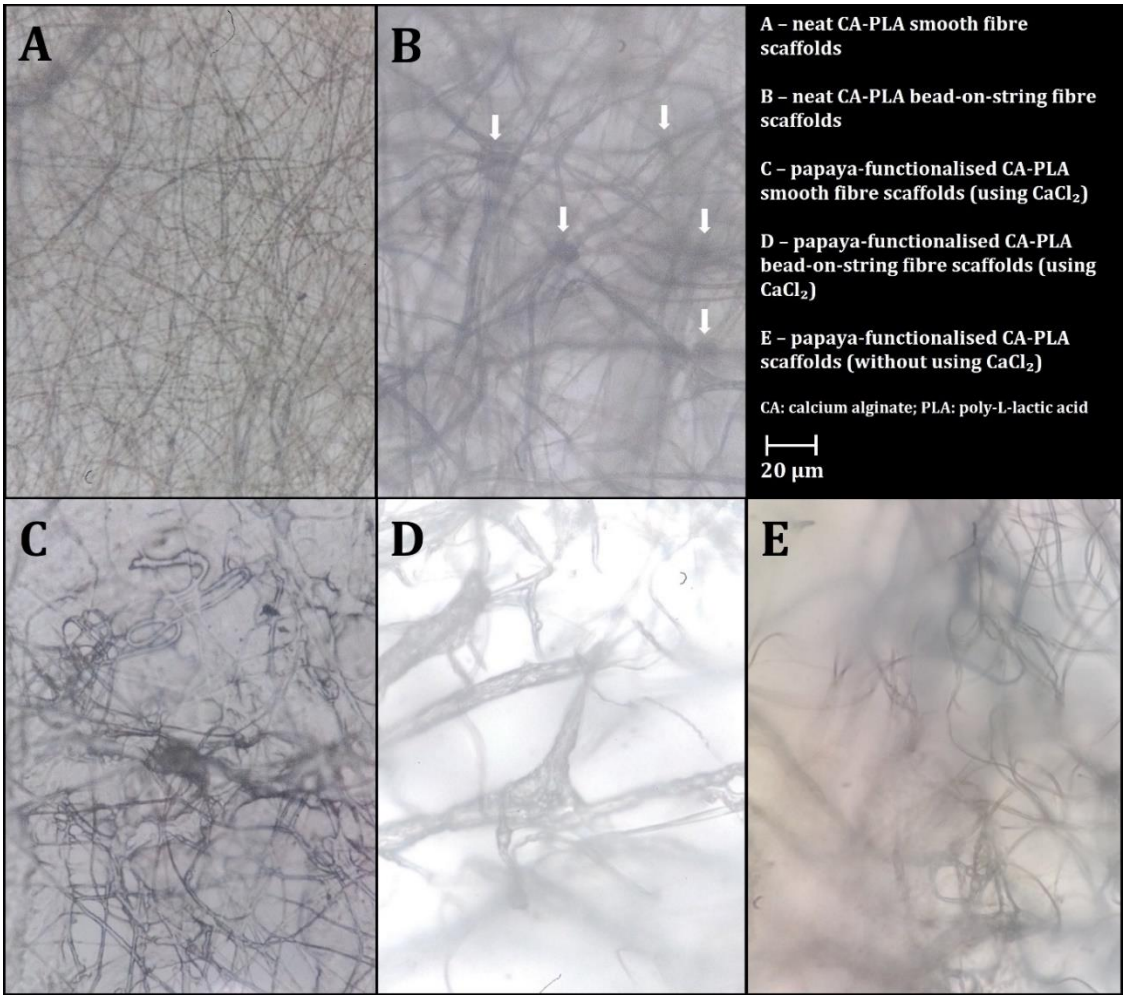


Figure 15: Microscopic appearance of electrospun scaffolds. Approximate diameters of fibres in the scaffolds are for A: ≤ 0.5 µm; B: ≤ 0.5 µm and 0.5–2 µm; C: 0.5–2 µm; D: 0.5–8 µm; and E: 0.5–2 µm. White arrows in panel B denote possible 'bead' formation. Images were acquired using a 100× oil immersion objective on an Olympus BX43 optical microscope.

A suggestion of bead-on-string fibres was evident in Figure 15B (i.e., scaffolds produced using the neat CA-PLA emulsion designed to do such), although they were infrequent and hard to definitively visualise. Furthermore, the fibres were not as smooth as in the neat CA-PLA scaffold in Figure 15A and had diameters ranging from ≤ 0.5 µm and 0.5–2 µm. The interior of the larger diameter fibres had an

irregular banded appearance, with some sections appearing more translucent than others. It is uncertain if this may also indicate bead formation, which may be noticeable at higher magnifications/resolutions, or whether it is simply a result of overlapping fibres. Qi et al. (2006), whose methodology was used in attempting to produce these bead-on-string fibres, generated bead-on-string CA-PLA fibres having diameters of approximately 1–1.5 μm in the 'string' aspect and 6.5–7.5 μm across the widest part of the spindle-shaped 'beads' when electrospun at 20 kV. Although, they utilised SEM in their analysis, beads of that diameter would have been visible through optical microscopy. Qi et al. (2006) used the anionic surfactant AOT, whereas the non-ionic surfactant Span60 was used in this experiment. Hu et al. (2015) investigated the effect of surfactant type in emulsion electrospinning and found that ionic surfactants increase conductivity thus producing fibres of a relatively smaller diameter, with the anionic surfactant sodium dodecyl sulfate producing the most uniform fibres. Interestingly, beads which were considered a flaw in that experiment, were observed when certain concentrations of the non-ionic surfactants Span80 and Pluronic F108 (polyethylene oxide–polypropylene oxide–polyethylene oxide triblock copolymer) were used. Thus, the differences between the fibres produced by Qi et al. (2006) and those produced in this experiment cannot be accounted for by difference in surfactant type. It is possible that the vertical electrospinning configuration used by Qi et al. (2006) allowed the 'beads' in the emulsion to fall into the spinneret needle, whereas the horizontal arrangement used in this study may have resulted in the CA beads settling to the base of the syringe, below the vicinity of the needle (Figure 16).

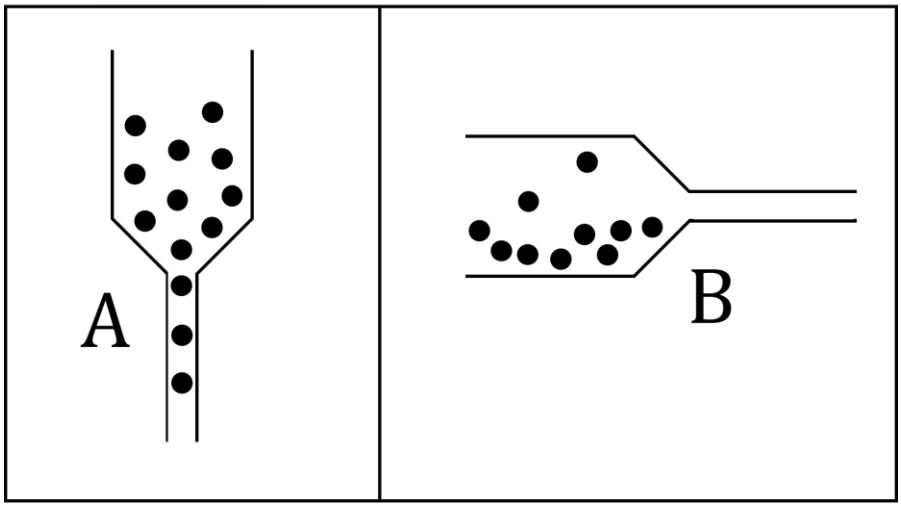


Figure 16: A: vertical electrospinning arrangement employed by Qi et al. (2006) in which CA beads in the emulsion can fall into the spinneret; B: horizontal electrospinning arrangement used in this study with the possibility of CA beads settling to the base of the syringe.

As can be seen in Figure 15C and Figure 15D, the papaya-functionalised CA-PLA scaffolds in which $CaCl_2$ was used both had wet appearances with fused webs. The emulsion designed to produce bead-on-string fibres had large fibres of 8 μm in diameter, although they appear to be a result of fusion of several microfiber strands. The papaya-functionalised CA-PLA scaffolds in which $CaCl_2$ was not used appeared less wet, however the fibres were not as uniform and had a greater size distribution when compared to the neat CA-PLA scaffolds. Furthermore, the pores between the papaya-functionalised fibres were larger and the overall scaffold appeared less matted. This likely translated into the fragility seen on the gross specimen (Figure 14E). Ahlawat et al. (2019) was able to obtain smooth, uniform papaya leaf extract-loaded PVA-gelatin nanofibers of diameters of 140±20 nm. While the obvious difference in polymer choices between that study and this experiment can be

considered, the mechanical structure of gelatin has been shown to improve in the absence of divalent ions such as Ca^{2+} (Xing et al., 2014). Thus, gelatin can be impacted similarly to alginate by the presence of calcium in papaya, although Ahlawat et al. (2019) did not detect calcium during their elemental analysis using EDX. Nevertheless, the impact of the Ca^{2+} present in papaya extract on the SA-PLA emulsion was recognised and accounted for in this experiment (see section 5.2). Optical microscopy of the final papaya extract used in this experiment revealed particles ranging in size from < 1 μm to 10 μm (Figure 17), despite being filtered through a syringe filter with 5 μm pore size prior to use. These particles were not seen on the oil-immersion blank and were seen to be in a state of constant Brownian motion, confirming their presence in the liquid extract. Ahlawat et al. (2019) performed transmission electron microscopy on their papaya leaf extract powder and found a particle size of 25±5.709 nm. It is possible that the micrometre impurities in our papaya extract may have contributed to the suboptimal fibre morphology. Interestingly, Balaji et al. (2016) used a papaya-extract like the one used in this experiment while electrospinning papaya- and honey-extract functionalised polyurethane fibres. However, they dissolved the aqueous papaya extract in N,N-dimethylformamide prior to incorporation into the electrospinning solution, and it is possible that dissolution in this organic solvent may have resulted in an extract with less impurities that is better incorporated into the organic-phase electrospinning solution.

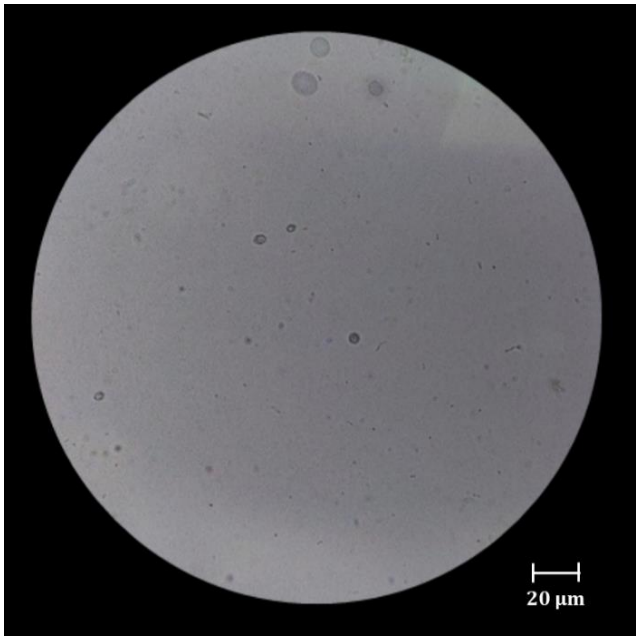


Figure 17: Microscopic appearance of the papaya extract, acquired using a 100× oil immersion objective on an Olympus BX43 microscope.

5.5 Future work and recommendations

It is evident that optimization of the papaya extract and the papaya-functionalised CA-PLA micro-fibrous scaffolds are needed. Attempting ethanol extraction of the papaya leaves and fruit, followed by roto-vaporisation can yield a solid extract that can be dissolved in aqueous solution, and possibly avoid large micrometre impurities. Similarly, dialysing the aqueous extract against a calcium-deficient buffer, using a dialysis pore size of < 1 kDa, can remove micrometre impurities and reduce Ca^{2+} levels in the extract while maintaining most bio-active constituents. A vertical electrospinning configuration can also be employed in attempting to produce bead-on-string fibres. Manipulation of ambient conditions and concentrations of polymers can also be done to optimise bead-on-string and smooth fibre formation, but this requires sufficient time to conduct which was

beyond the timeline of this current experiment. Assessment of the release profile of papaya extract from the scaffolds are to be undertaken by immersing 20 mg of the scaffolds in 3 mL of phosphate-buffered saline (PBS), and then at predetermined time intervals (over a 1–2 week period) taking 2 mL of the supernatant and performing UV-vis spectroscopy to assess for absorbance specific to the papaya extract. 2 mL of fresh PBS will have to be replaced every time samples for analysis are taken. The goal will be to perform further physiochemical characterisations such as electron microscopy, and eventually perform in vivo testing of the papaya-functionalised scaffolds in excision wound models in rats.

6. Conclusion

Chronic wound care remains an issue of paramount clinical importance, but also a potential area for entrepreneurial development. The fruit and leaves of the Carica papaya Linn tree possess proteolytic enzymes (papain and chymopapain) that aid in the initial debridement of sloughy and necrotic wounds. Its phytochemicals including flavonoids, alkaloids, glycosides, saponins, tannins, sterols, carotenoids, and phenolics confer antioxidant, anti-inflammatory, and antimicrobial properties that carry chronic wounds through the inflammatory phase and into the proliferative phase of wound healing. Vitamin C is also present and promotes collagen synthesis essential for granulation tissue.

Micro/nano-fibrous dressings mimic ECM and encourage cellular adhesion and integration. Furthermore, they provide a high surface area-to-volume ratio to promote haemostasis and allow functionalisation. They have good porosity to allow adequate oxygenation and fluid exudation, yet still prevent excess desiccation and microbial invasion. Electrospinning is a versatile technique to produce these scaffolds, in which natural (e.g., alginates from brown seaweed) and bio-derived synthetic (e.g., PLA from carbohydrate food groups such as cassava and sugar cane) polymers can be utilised. Furthermore, electrospinning has the potential to be scaled to industrial production levels.

In this experiment, emulsion electrospinning of neat water-in-oil emulsions of SA solution and PLA in chloroform, using Span60 surfactant, was undertaken using a simple set-up. The obtained scaffolds were immersed in $CaCl_2$ solution to convert

soluble SA to insoluble CA. Uniform smooth micro-fibrous scaffolds (diameters ≤ 0.5 μm) were observed on optical microscopy. Attempts to produce bead-on-string fibres through replacement of Na^{+} with Ca^{2+} in alginate prior to electrospinning were inconclusive, with only sparse bead formation being noticed. An aqueous extract of papaya leaves, seeds, and epicarp was obtained; and incorporated into the emulsions prior to electrospinning. It was discovered that our papaya extract contained Ca^{2+} (measured at 1.16 $mmol.L^{-1}$) and produced insoluble CA when combined with the alginate solution prior to emulsification. This prevented creation of a homogeneous emulsion with ≤ 1.0 mm firm papaya-incorporated CA globules clogging the needle during electrospinning. Thus, papaya extract was added to the SA-PLA emulsion just prior to electrospinning producing a more uniform emulsion which electrospun without clogging. This papaya-functionalised CA-PLA electrospun scaffold had fibres with diameters of 0.5–2 μm, however its gross structure as a membrane was fragile and tore easily (in comparison to neat CA-PLA scaffolds). Persistence of ≤ 10 μm particulates in the papaya extract may have contributed to its fragility. Overall, this is promising evidence that papaya-functionalised CA-PLA electrospun scaffolds can be generated, but optimisation of the technique is still needed.

7. References

Abrigo, M., McArthur, S. L., & Kingshott, P. (2014). Electrospun Nanofibers as Dressings for Chronic Wound Care: Advances, Challenges, and Future Prospects. *Macromolecular Bioscience*, *14*(6), 772-792. https://doi.org/10.1002/mabi.201300561

AdvaCare Pharma. (2022). *Alginate Dressing (StayGuard™)*. AdvaCare Pharma USA. Retrieved 30th January 2022 from https://www.advacarepharma.com/en/medical-devices/alginate-dressing

Afshar, S., Rashedi, S., Nazockdast, H., & Ghazalian, M. (2019). Preparation and characterization of electrospun poly(lactic acid)-chitosan core-shell nanofibers with a new solvent system. *International Journal of Biological Macromolecules*, *138*, 1130-1137. https://doi.org/https://doi.org/10.1016/j.ijbiomac.2019.07.053

Ahlawat, J., Kumar, V., & Gopinath, P. (2019). Carica papaya loaded poly (vinyl alcohol)-gelatin nanofibrous scaffold for potential application in wound dressing. *103*, 109834. http://www.sciencedirect.com/science/article/pii/S0928493117345678

Angeles, M., Cheng, H.-L., & Velankar, S. S. (2008). Emulsion electrospinning: composite fibers from drop breakup during electrospinning. *Polymers for Advanced Technologies*, *19*(7), 728-733. https://doi.org/10.1002/pat.1031

Asghar, N., Naqvi, S. A. R., Hussain, Z., Rasool, N., Khan, Z. A., Shahzad, S. A., Sherazi, T. A., Janjua, M. R. S. A., Nagra, S. A., Zia-Ul-Haq, M., & Jaafar, H. Z. (2016). Compositional difference in antioxidant and antibacterial activity of all parts

of the Carica papaya using different solvents. *Chemistry Central journal*, *10*, 5-5. https://doi.org/10.1186/s13065-016-0149-0

Azimi, B., Maleki, H., Zavagna, L., De la Ossa, J. G., Linari, S., Lazzeri, A., & Danti, S. (2020). Bio-Based Electrospun Fibers for Wound Healing. *Journal of functional biomaterials*, *11*(3), 67. https://doi.org/10.3390/jfb11030067

Bae, H.-S., Haider, A., Selim, K., Kang, D.-Y., Kim, E.-J., & Kang, I.-K. (2013). Fabrication of highly porous PMMA electrospun fibers and their application in the removal of phenol and iodine. *Journal of Polymer Research*, *20*. https://doi.org/10.1007/s10965-013-0158-9

Balaji, A., Jaganathan, S. K., Ismail, A. F., & Rajasekar, R. (2016). Fabrication and hemocompatibility assessment of novel polyurethane-based bio-nanofibrous dressing loaded with honey and Carica papaya extract for the management of burn injuries. *International journal of nanomedicine*, *11*, 4339-4355. https://doi.org/10.2147/ijn.S112265

Bhardwaj, N., & Kundu, S. C. (2010). Electrospinning: A fascinating fiber fabrication technique. *Biotechnology Advances*, *28*(3), 325-347. https://doi.org/https://doi.org/10.1016/j.biotechadv.2010.01.004

Boer, M., Duchnik, E., Maleszka, R., & Marchlewicz, M. (2016). Structural and biophysical characteristics of human skin in maintaining proper epidermal barrier function. *Postepy dermatologii i alergologii*, *33*(1), 1-5. https://doi.org/10.5114/pdia.2015.48037

Bonino, C. A., Krebs, M. D., Saquing, C. D., Jeong, S. I., Shearer, K. L., Alsberg, E., & Khan, S. A. (2011). Electrospinning alginate-based nanofibers: From blends to crosslinked low molecular weight alginate-only systems. *Carbohydrate*

Polymers, *85*(1), 111-119. https://doi.org/https://doi.org/10.1016/j.carbpol.2011.02.002

Casalini, T., Rossi, F., Castrovinci, A., & Perale, G. (2019). A Perspective on Polylactic Acid-Based Polymers Use for Nanoparticles Synthesis and Applications [Review]. *Frontiers in Bioengineering and Biotechnology*, *7*(259). https://doi.org/10.3389/fbioe.2019.00259

Casper, C. L., Stephens, J. S., Tassi, N. G., Chase, D. B., & Rabolt, J. F. (2004). Controlling Surface Morphology of Electrospun Polystyrene Fibers: Effect of Humidity and Molecular Weight in the Electrospinning Process. *Macromolecules*, *37*(2), 573-578. https://doi.org/10.1021/ma0351975

Caterson, E. J., Li, W. J., Nesti, L. J., Albert, T., Danielson, K., & Tuan, R. S. (2002). Polymer/Alginate Amalgam for Cartilage- Tissue Engineering. *Annals of the New York Academy of Sciences*, *961*(1), 134-138. https://doi.org/10.1111/j.1749-6632.2002.tb03066.x

Cawich, S. O., Islam, S., Hariharan, S., Harnarayan, P., Budhooram, S., Ramsewak, S., & Naraynsingh, V. (2014). The Economic Impact of Hospitalization for Diabetic Foot Infections in a Caribbean Nation. *The Permanente Journal*, *18*(1), e101–e104. http://doi.org/10.7812/TPP/13-096

Chou, S.-F., Carson, D., & Woodrow, K. A. (2015). Current strategies for sustaining drug release from electrospun nanofibers. *Journal of Controlled Release*, *220*, 584-591. https://doi.org/https://doi.org/10.1016/j.jconrel.2015.09.008

da Silva, D., Kaduri, M., Poley, M., Adir, O., Krinsky, N., Shainsky-Roitman, J., & Schroeder, A. (2018). Biocompatibility, biodegradation and excretion of polylactic acid (PLA) in medical implants and theranostic systems. *Chemical*

Engineering Journal, *340*, 9-14. https://doi.org/https://doi.org/10.1016/j.cej.2018.01.010

Dawkins, G., Hewitt, H., Wint, Y., Obiefuna, P. C., & Wint, B. (2003). Antibacterial effects of Carica papaya fruit on common wound organisms. *West Indian Med J*, *52*(4), 290-292.

Deitzel, J. M., Kleinmeyer, J., Harris, D., & Beck Tan, N. C. (2001). The effect of processing variables on the morphology of electrospun nanofibers and textiles. *Polymer*, *42*(1), 261-272. https://doi.org/https://doi.org/10.1016/S0032-3861(00)00250-0

Deitzel, J. M., Kleinmeyer, J. D., Hirvonen, J. K., & Beck Tan, N. C. (2001). Controlled deposition of electrospun poly(ethylene oxide) fibers. *Polymer*, *42*(19), 8163-8170. https://doi.org/https://doi.org/10.1016/S0032-3861(01)00336-6

Dhivya, S., Padma, V. V., & Santhini, E. (2015). Wound dressings - a review. *BioMedicine*, *5*(4), 22-22. https://doi.org/10.7603/s40681-015-0022-9

Dwivedi, M. K., Sonter, S., Mishra, S., Patel, D. K., & Singh, P. K. (2020). Antioxidant, antibacterial activity, and phytochemical characterization of Carica papaya flowers. *Beni-Suef University Journal of Basic and Applied Sciences*, *9*(1), 23. https://doi.org/10.1186/s43088-020-00048-w

Elsner, J. J., Kraitzer, A., Grinberg, O., & Zilberman, M. (2012). Highly porous drug-eluting structures: from wound dressings to stents and scaffolds for tissue regeneration. *Biomatter*, *2*(4), 239-270. https://doi.org/10.4161/biom.22838

Eming, S. A., Martin, P., & Tomic-Canic, M. (2014). Wound repair and regeneration: mechanisms, signaling, and translation. *Science translational medicine*,

6(265), 265sr266-265sr266. https://doi.org/10.1126/scitranslmed.3009337

Fatehi, P., & Abbasi, M. (2020). Medicinal plants used in wound dressings made of electrospun nanofibers [https://doi.org/10.1002/term.3119]. *Journal of Tissue Engineering and Regenerative Medicine*, *14*(11), 1527-1548. https://doi.org/https://doi.org/10.1002/term.3119

Fatima, U., & Shahid, S. (2018). Pharmacological Activities of Carica papaya Linn. *Journal of Basic & Applied Sciences*, *14*, 210-216. https://doi.org/10.6000/1927-5129.2018.14.33

Feng, X., Li, J., Zhang, X., Liu, T., Ding, J., & Chen, X. (2019). Electrospun polymer micro/nanofibers as pharmaceutical repositories for healthcare. *Journal of Controlled Release*, *302*, 19-41. https://doi.org/https://doi.org/10.1016/j.jconrel.2019.03.020

Ferrall-Fairbanks, M. C., Kieslich, C. A., & Platt, M. O. (2020). Reassessing enzyme kinetics: Considering protease-as-substrate interactions in proteolytic networks. *Proceedings of the National Academy of Sciences*, *117*(6), 3307. https://doi.org/10.1073/pnas.1912207117

Fong, H., Chun, I., & Reneker, D. H. (1999). Beaded nanofibers formed during electrospinning. *Polymer*, *40*(16), 4585-4592. https://doi.org/https://doi.org/10.1016/S0032-3861(99)00068-3

Frykberg, R. G., & Banks, J. (2015). Challenges in the Treatment of Chronic Wounds. *Advances in wound care*, *4*(9), 560-582. https://doi.org/10.1089/wound.2015.0635

Galeano, M., Torre, V., Deodato, B., Campo, G. M., Colonna, M., Sturiale, A., Squadrito, F., Cavallari, V., Cucinotta, D., Buemi, M., & Altavilla, D. (2001). Raxofelast, a

hydrophilic vitamin E-like antioxidant, stimulates wound healing in genetically diabetic mice. *Surgery*, *129*(4), 467-477. https://doi.org/10.1067/msy.2001.112072

Ghosal, K., Agatemor, C., Tucker, N., Kny, E., & Thomas, S. (2018). CHAPTER 1 Electrical Spinning to Electrospinning: a Brief History. In *Electrospinning: From Basic Research to Commercialization* (pp. 1-23). The Royal Society of Chemistry. https://doi.org/10.1039/9781788012942-00001

Gizaw, M., Thompson, J., Faglie, A., Lee, S.-Y., Neuenschwander, P., & Chou, S.-F. (2018). Electrospun Fibers as a Dressing Material for Drug and Biological Agent Delivery in Wound Healing Applications. *Bioengineering (Basel, Switzerland)*, *5*(1), 9. https://doi.org/10.3390/bioengineering5010009

Gomes, D. S., da Silva, A. N. R., Morimoto, N. I., Mendes, L. T. F., Furlan, R., & Ramos, I. (2007). Characterization of an electrospinning process using different PAN/DMF concentrations. *Polímeros: Ciência e Tecnologia*, *17*(3), 206-211. https://www.redalyc.org/articulo.oa?id=47017308 (IN FILE)

Gómez-Pachón, E. Y., Vera-Graziano, R., & Campos, R. M. (2014). Structure of poly(lactic-acid) PLA nanofibers scaffolds prepared by electrospinning. *IOP Conference Series: Materials Science and Engineering*, *59*, 012003. https://doi.org/10.1088/1757-899x/59/1/012003

Government of the Republic of Trinidad and Tobago. (2012). *Trinidad and Tobago chronic non-communicable disease risk factor survey (Pan American STEPS)*. Ministry of Health Government of the Republic of Trinidad and Tobago

Han, G., & Ceilley, R. (2017). Chronic Wound Healing: A Review of Current Management and Treatments. *Advances in therapy*, *34*(3), 599-610. https://doi.org/10.1007/s12325-017-0478-y

He, H., Kara, Y., & Molnar, K. (2019). Effect of needle characteristic on fibrous PEO produced by electrospinning. *Resolution and Discovery*, *4*(1), 7-11. https://doi.org/10.1556/2051.2018.00063

Hu, J., Prabhakaran, M. P., Ding, X., & Ramakrishna, S. (2015). Emulsion electrospinning of polycaprolactone: influence of surfactant type towards the scaffold properties. *Journal of Biomaterials Science, Polymer Edition*, *26*(1), 57-75. https://doi.org/10.1080/09205063.2014.982241

Hu, X., Liu, S., Zhou, G., Huang, Y., Xie, Z., & Jing, X. (2014). Electrospinning of polymeric nanofibers for drug delivery applications. *Journal of Controlled Release*, *185*, 12-21. https://doi.org/https://doi.org/10.1016/j.jconrel.2014.04.018

Huang, C., & Thomas, N. L. (2020). Fabrication of porous fibers via electrospinning: strategies and applications. *Polymer Reviews*, *60*(4), 595-647. https://doi.org/10.1080/15583724.2019.1688830

Hunt, T. K., & Hopf, H. W. (1997). Wound healing and wound infection: what surgeons and anesthesiologists can do. *Surgical Clinics of North America*, *77*(3), 587-606.

Hussain, F., Khurshid, M. F., Masood, R., & Ibrahim, W. (2017). Developing antimicrobial calcium alginate fibres from neem and papaya leaves extract. *Journal of Wound Care*, *26*(12), 778-783. https://doi.org/10.12968/jowc.2017.26.12.778

Jayarajan, R., Narayanan, P., & Adenwalla, H. (2016). Papaya pulp for enzymatic wound debridement in burns. *Indian Journal of Burns*, *24*(1), 24-28. http://www.ijburns.com/article.asp?issn=0971-653X

Jones, V., Grey, J. E., & Harding, K. G. (2006). Wound dressings. *BMJ (Clinical research ed.)*, *332*(7544), 777-780. https://doi.org/10.1136/bmj.332.7544.777

Junqueira, L. C. U. a. M. A. L. (2010). Junqueira's basic histology : text and atlas.

Kanmaz, D., Toprakci, H. A. K., Olmez, H., & Toprakci, O. (2018). Electrospun Polylactic Acid Based Nanofibers for Biomedical Applications. *Material Science Research India*, *15*(3), 16. https://doi.org/http://dx.doi.org/10.13005/msri/150304

Kharaghani, D., Gitigard, P., Ohtani, H., Kim, K. O., Ullah, S., Saito, Y., Khan, M. Q., & Kim, I. S. (2019). Design and characterization of dual drug delivery based on in-situ assembled PVA/PAN core-shell nanofibers for wound dressing application. *Scientific Reports*, *9*(1), 12640. https://doi.org/10.1038/s41598-019-49132-x

Kim, K. W., Lee, K. H., Khil, M. S., Ho, Y. S., & Kim, H. Y. (2004). The effect of molecular weight and the linear velocity of drum surface on the properties of electrospun poly(ethylene terephthalate) nonwovens. *Fibers and Polymers*, *5*(2), 122-127. https://doi.org/10.1007/BF02902925

Kong, Y. R., Jong, Y. X., Balakrishnan, M., Bok, Z. K., Weng, J. K. K., Tay, K. C., Goh, B. H., Ong, Y. S., Chan, K. G., Lee, L. H., & Khaw, K. Y. (2021). Beneficial Role of Carica papaya Extracts and Phytochemicals on Oxidative Stress and Related Diseases: A Mini Review. *Biology*, *10*(4), 287. https://doi.org/10.3390/biology10040287

Kriel, H. C., M; Smit, E. (2015). *Enabling breakthrough technologies using nanofiber expertise*. International Fiber Journal. Retrieved 20th January 2022 from https://fiberjournal.com/enabling-breakthrough-technologies-using-nanofiber-expertise-2/

Krisp, C., Jacobsen, F., McKay, M. J., Molloy, M. P., Steinstraesser, L., & Wolters, D. A. (2013). Proteome analysis reveals antiangiogenic environments in chronic wounds of diabetes mellitus type 2 patients [https://doi.org/10.1002/pmic.201200502]. *PROTEOMICS*, *13*(17), 2670-2681. https://doi.org/https://doi.org/10.1002/pmic.201200502

Kumar, V. A. A. K. A. J. C. R. S. L. (2013). *Robbins basic pathology*. Elsevier/Saunders.

Kyzioł, A., Michna, J., Moreno, I., Gamez, E., & Irusta, S. (2017). Preparation and characterization of electrospun alginate nanofibers loaded with ciprofloxacin hydrochloride. *European Polymer Journal*, *96*, 350-360. https://doi.org/https://doi.org/10.1016/j.eurpolymj.2017.09.020

Lauer, G., Sollberg, S., Cole, M., Krieg, T., Eming, S. A., Flamme, I., Stürzebecher, J., & Mann, K. (2000). Expression and Proteolysis of Vascular Endothelial Growth Factor is Increased in Chronic Wounds. *Journal of Investigative Dermatology*, *115*(1), 12-18. https://doi.org/10.1046/j.1523-1747.2000.00036.x

Lee, K. Y., & Mooney, D. J. (2012). Alginate: properties and biomedical applications. *Progress in polymer science*, *37*(1), 106-126. https://doi.org/10.1016/j.progpolymsci.2011.06.003

Li, D., Wang, Y., & Xia, Y. (2003). Electrospinning of Polymeric and Ceramic Nanofibers as Uniaxially Aligned Arrays. *Nano Letters*, *3*(8), 1167-1171. https://doi.org/10.1021/nl0344256

Li, T., Ding, X., Tian, L., Hu, J., Yang, X., & Ramakrishna, S. (2017). The control of beads diameter of bead-on-string electrospun nanofibers and the corresponding release behaviors of embedded drugs. *Materials Science and Engineering: C*, *74*, 471-477. https://doi.org/https://doi.org/10.1016/j.msec.2016.12.050

Liu, X., Xu, H., Zhang, M., & Yu, D.-G. (2021). Electrospun Medicated Nanofibers for Wound Healing: Review. *Membranes*, *11*(10). https://doi.org/10.3390/membranes11100770

MacKay, D., & Miller, A. L. Nutritional support for wound healing. (1089-5159 (Print)).

Marfo, E. K., Oke, O. L., & Afolabi, O. A. (1986). Chemical composition of papaya (Carica papaya) seeds. *Food Chemistry*, *22*(4), 259-266. https://doi.org/https://doi.org/10.1016/0308-8146(86)90084-1

Matabola, K. P., & Moutloali, R. M. (2013). The influence of electrospinning parameters on the morphology and diameter of poly(vinyledene fluoride) nanofibers- effect of sodium chloride. *Journal of Materials Science*, *48*(16), 5475-5482. https://doi.org/10.1007/s10853-013-7341-6

McCarty, S. M., & Percival, S. L. (2013). Proteases and Delayed Wound Healing. *Advances in wound care*, *2*(8), 438-447. https://doi.org/10.1089/wound.2012.0370

Migliaresi, C. R., GA; Volpato, FZ; Zeni, D. (2012). Advanced Electrospinning Setups and Special Fibre and Mesh Morphologies. In N. M. Neves (Ed.), *Electrospinning for Advanced Biomedical Applications and Therapies* (pp. 23-68). Smithers Rapra Technology Ltd. https://pdf.zlibcdn.com/dtoken/386654b3e4f6e74d730401054b1f7890/Electrospinning for Advanced Biomedical Applicatio 2316946 (z-lib.org).pdf

Mikhal'chik, E. V., Ivanova, A. V., Anurov, M. V., Titkova, S. M., Pen'kov, L. Y., Kharaeva, Z. F., & Korkina, L. G. (2004). Wound-healing effect of papaya-

based preparation in experimental thermal trauma. *Bull Exp Biol Med*, *137*(6), 560-562. https://doi.org/10.1023/b:bebm.0000042711.31775.f7

Miroshnichenko, S., Timofeeva, V., Permykova, E., Ershov, S., Kiryukhantsev-Korneev, P., Dvořaková, E., Shtansky, D. V., Zajíčková, L., Solovieva, A., & Manakhov, A. (2019). Plasma-Coated Polycaprolactone Nanofibers with Covalently Bonded Platelet-Rich Plasma Enhance Adhesion and Growth of Human Fibroblasts. *Nanomaterials (Basel, Switzerland)*, *9*(4), 637. https://doi.org/10.3390/nano9040637

Mit-uppatham, C., Nithitanakul, M., & Supaphol, P. (2004). Ultrafine Electrospun Polyamide-6 Fibers: Effect of Solution Conditions on Morphology and Average Fiber Diameter [https://doi.org/10.1002/macp.200400225]. *Macromolecular Chemistry and Physics*, *205*(17), 2327-2338. https://doi.org/https://doi.org/10.1002/macp.200400225

Mohammadian, F., & Eatemadi, A. (2017). Drug loading and delivery using nanofibers scaffolds. *Artificial Cells, Nanomedicine, and Biotechnology*, *45*(5), 881-888. https://doi.org/10.1080/21691401.2016.1185726

Murthy, M. B., Murthy, B. K., & Bhave, S. (2012). Comparison of safety and efficacy of papaya dressing with hydrogen peroxide solution on wound bed preparation in patients with wound gape. *Indian journal of pharmacology*, *44*(6), 784-787. https://www.ncbi.nlm.nih.gov/pubmed/23248412

https://www.ncbi.nlm.nih.gov/pmc/articles/PMC3523510/

Nafiu, A. B., & Rahman, M. T. (2015). Anti-inflammatory and antioxidant properties of unripe papaya extract in an excision wound model. *Pharmaceutical Biology*, *53*(5), 662-671. https://doi.org/10.3109/13880209.2014.936470

National Center for Biotechnology Information. (2022). *PubChem Compound Summary for CID 6212, Chloroform.* National Library of Medicine (US), National Center for Biotechnology Information. Retrieved 20 January 2022 from https://pubchem.ncbi.nlm.nih.gov/compound/Chloroform

Nayak, B. S., Ramdeen, R., Adogwa, A., Ramsubhag, A., & Marshall, J. R. (2012). Wound-healing potential of an ethanol extract of Carica papaya (Caricaceae) seeds. *International Wound Journal*, *9*(6), 650-655. https://doi.org/10.1111/j.1742-481X.2011.00933.x

Nayak, S. B., Pinto Pereira, L., & Maharaj, D. (2007). Wound healing activity of Carica papaya L. in experimentally induced diabetic rats. *Indian J Exp Biol*, *45*(8), 739-743. http://dx.doi.org/

Nie, H., Ho, M.-L., Wang, C.-K., Wang, C.-H., & Fu, Y.-C. (2009). BMP-2 plasmid loaded PLGA/HAp composite scaffolds for treatment of bone defects in nude mice. *Biomaterials*, *30*(5), 892-901. https://doi.org/https://doi.org/10.1016/j.biomaterials.2008.10.029

Nugroho, A., Heryani, H., Choi, J. S., & Park, H.-J. (2017). Identification and quantification of flavonoids in Carica papaya leaf and peroxynitrite-scavenging activity. *Asian Pacific Journal of Tropical Biomedicine*, *7*(3), 208-213. https://doi.org/https://doi.org/10.1016/j.apjtb.2016.12.009

Nwofia, G., Ojimelukwe, P., & Eji, C. (2012). Chemical composition of leaves, fruit pulp and seeds in some Carica papaya (L) morphotypes. *International Journal of Medicinal and Aromatic Plants*, *2*(1), 200-206. https://www.researchgate.net/publication/236646755_Chemical_composition_of_leaves_fruit_pulp_and_seeds_in_some_Carica_papaya_L_morphotypes

OECD. (2005). *Consensus Document on the Biology of Papaya (Carica papaya)* (Series on Harmonisation of Regulatory Oversight in Biotechnology No. 33, Issue. O. f. E. C.-o. a. Development. https://www.oecd.org/env/ehs/biotrack/46815818.pdf

Pandey, S., Cabot, P. J., Shaw, P. N., & Hewavitharana, A. K. (2016). Anti-inflammatory and immunomodulatory properties of Carica papaya. *Journal of Immunotoxicology*, *13*(4), 590-602. https://doi.org/10.3109/1547691X.2016.1149528

Qi, H., Hu, P., Xu, J., & Wang, A. (2006). Encapsulation of Drug Reservoirs in Fibers by Emulsion Electrospinning: Morphology Characterization and Preliminary Release Assessment. *Biomacromolecules*, *7*(8), 2327-2330. https://doi.org/10.1021/bm060264z

Rajendran, N. K., Kumar, S. S. D., Houreld, N. N., & Abrahamse, H. (2018). A review on nanoparticle based treatment for wound healing. *Journal of Drug Delivery Science and Technology*, *44*, 421-430. https://doi.org/10.1016/j.jddst.2018.01.009

Rambaran, K., Teelucksingh, S., Gowrie Sankar, S., Boyne, M., Xuereb, G., Giorgetti, A., & Zimmermann, M. B. (2021). High prevalence of childhood overweight and obesity in ten Caribbean countries: 2018 cross-sectional data and a narrative review of trends in Trinidad and Tobago. *Child and Adolescent Obesity*, *4*(1), 23-36. https://doi.org/10.1080/2574254X.2020.1847632

Ramesh, B., Cherian, K. M., & Fakoya, A. O. J. (2020). Fabrication and Electrospinning of 3D Biodegradable Poly-l-Lactic Acid (PLLA) Nanofibers for Clinical Application. In K. Turksen (Ed.), *Stem Cell Nanotechnology: Methods and*

Protocols (pp. 119-128). Springer US. https://doi.org/10.1007/7651_2019_213

Sahay, R., Thavasi, V., & Ramakrishna, S. (2011). Design Modifications in Electrospinning Setup for Advanced Applications. *Journal of Nanomaterials*, *2011*, 317673. https://doi.org/10.1155/2011/317673

Sawawi, M., Sahari, S. K., Kuan, N., Yusof, M., Andew, M., Salleh, S. F., & Sapawi, R. (2017). Optimisation of electrospinning parameter for Poly(L-lactic) acid (PLLA) electrospun nanofiber [10.1051/matecconf/20178702012]. *MATEC Web Conf.*, *87*. https://doi.org/10.1051/matecconf/20178702012

Schultz, G. S., Sibbald, R. G., Falanga, V., Ayello, E. A., Dowsett, C., Harding, K., Romanelli, M., Stacey, M. C., Teot, L., & Vanscheidt, W. (2003). Wound bed preparation: a systematic approach to wound management [https://doi.org/10.1046/j.1524-475X.11.s2.1.x]. *Wound Repair and Regeneration*, *11*(s1), S1-S28. https://doi.org/https://doi.org/10.1046/j.1524-475X.11.s2.1.x

Sheffield, P. J. (1988). Problem Wounds: The role of oxygen. *Tissue oxygen measurement*, 17-51.

Singh, U., Mohan, S., Davis, F., & Mitchell, G. (2018). Modifying the thermomechanical properties of electrospun fibres of poly-vinyl cinnamate by photo-cross-linking. *SN Applied Sciences*, *1*(1), 31. https://doi.org/10.1007/s42452-018-0033-8

Soares, R. M. D., Siqueira, N. M., Prabhakaram, M. P., & Ramakrishna, S. (2018). Electrospinning and electrospray of bio-based and natural polymers for biomaterials development. *Materials Science and Engineering: C*, *92*, 969-982. https://doi.org/https://doi.org/10.1016/j.msec.2018.08.004

Sousa Coelho, D., Veleirinho, B., Alberti, T., Maestri, A., Yunes, R., Dias, P., & Maraschin, M. (2018). Electrospinning Technology: Designing Nanofibers toward Wound Healing Application. In. https://doi.org/10.5772/intechopen.81530

Stanley, A., & Osler, T. (2001). Senescence and the healing rates of venous ulcers. *Journal of Vascular Surgery*, *33*(6), 1206-1211. https://doi.org/10.1067/mva.2001.115379

Stellenbosch Nanofiber Company. (2017). *Stellenbosch Nanofiber Company*. Retrieved 20th January 2022 from https://sncfibers.com/

Stocco, T. D., Bassous, N. J., Zhao, S., Granato, A. E. C., Webster, T. J., & Lobo, A. O. (2018). Nanofibrous scaffolds for biomedical applications [10.1039/C8NR02002G]. *Nanoscale*, *10*(26), 12228-12255. https://doi.org/10.1039/C8NR02002G

Sullivan, J. V., & Myers, S. (2022). 1 - Skin Structure and Function, Wound Healing and Scarring. In R. D. Farhadieh, N. W. Bulstrode, B. J. Mehrara, & S. Cugno (Eds.), *Plastic Surgery - Principles and Practice* (pp. 1-14). Elsevier. https://doi.org/https://doi.org/10.1016/B978-0-323-65381-7.00001-0

Tam, S. K., Dusseault, J., Bilodeau, S., Langlois, G., Hallé, J.-P., & Yahia, L. H. (2011). Factors influencing alginate gel biocompatibility. *Journal of Biomedical Materials Research Part A*, *98A*(1), 40-52. https://doi.org/10.1002/jbm.a.33047

Taylor, G. I., & Van Dyke, M. D. (1969). Electrically driven jets. *Proceedings of the Royal Society of London. A. Mathematical and Physical Sciences*, *313*(1515), 453-475. https://doi.org/10.1098/rspa.1969.0205

Taylor, G. I. S. (1964). Disintegration of water drops in an electric field. *Proceedings of the Royal Society of London. Series A. Mathematical and Physical Sciences*, *280*, 383 - 397.

Telgenhoff, D., & Shroot, B. (2005). Cellular senescence mechanisms in chronic wound healing. *Cell Death & Differentiation*, *12*(7), 695-698. https://doi.org/10.1038/sj.cdd.4401632

Teo, W. E., & Ramakrishna, S. (2006). A review on electrospinning design and nanofibre assemblies. *Nanotechnology*, *17*(14), R89-R106. https://doi.org/10.1088/0957-4484/17/14/r01

Triticum. (2012). L-Mesitran®. In. Netherlands: Triticum Exploitatie B.V.

Tucker, N., Stanger, J. J., Staiger, M. P., Razzaq, H., & Hofman, K. (2012). The History of the Science and Technology of Electrospinning from 1600 to 1995. *Journal of Engineered Fibers and Fabrics*, *7*(2_suppl), 155892501200702S155892501200710. https://doi.org/10.1177/155892501200702S10

Vandeputte, J. (2003). *Honey Based-Skin Care Preparation* (Netherlands Patent No. W. I. P. Organization. https://worldwide.espacenet.com/publicationDetails/biblio?II=3&ND=3&adjacent=true&locale=en_EP&FT=D&date=20120913&CC=PT&NR=1515734E&KC=E#

Vasuki, V., Thanmaran, N., Vimalakaran, B., & Madan, K. (2017). Comparative study of papaya dressing versus normal saline dressing in healing of ulcers [Original Research Articles]. *4*(4), 1209-1216. https://doi.org/https://www.ijsurgery.com/index.php/isj/article/view/1108

Veleirinho, B., Rei, M. F., & Lopes-Da-Silva, J. A. (2008). Solvent and concentration effects on the properties of electrospun poly(ethylene terephthalate) nanofiber mats [https://doi.org/10.1002/polb.21380]. *Journal of Polymer Science Part B: Polymer Physics*, *46*(5), 460-471. https://doi.org/https://doi.org/10.1002/polb.21380

Wang, C., Yan, K.-W., Lin, Y.-D., & Hsieh, P. C. H. (2010). Biodegradable Core/Shell Fibers by Coaxial Electrospinning: Processing, Fiber Characterization, and Its Application in Sustained Drug Release. *Macromolecules*, *43*(15), 6389-6397. https://doi.org/10.1021/ma100423x

Wannatong, L., Sirivat, A., & Supaphol, P. (2004). Effects of solvents on electrospun polymeric fibers: preliminary study on polystyrene [https://doi.org/10.1002/pi.1599]. *Polymer International*, *53*(11), 1851-1859. https://doi.org/https://doi.org/10.1002/pi.1599

Wayne, J. S., McDowell, C. L., Shields, K. J., & Tuan, R. S. (2005). In Vivo Response of Polylactic Acid–Alginate Scaffolds and Bone Marrow-Derived Cells for Cartilage Tissue Engineering. *Tissue Engineering*, *11*(5-6), 953-963. https://doi.org/10.1089/ten.2005.11.953

Xing, Q., Yates, K., Vogt, C., Qian, Z., Frost, M. C., & Zhao, F. (2014). Increasing Mechanical Strength of Gelatin Hydrogels by Divalent Metal Ion Removal. *Scientific Reports*, *4*(1), 4706. https://doi.org/10.1038/srep04706

Xu, W., Shen, R., Yan, Y., & Gao, J. (2017). Preparation and characterization of electrospun alginate/PLA nanofibers as tissue engineering material by emulsion eletrospinning. *Journal of the Mechanical Behavior of Biomedical Materials*, *65*, 428-438. https://doi.org/https://doi.org/10.1016/j.jmbbm.2016.09.012

Xue, J., Wu, T., Dai, Y., & Xia, Y. (2019). Electrospinning and Electrospun Nanofibers: Methods, Materials, and Applications. *Chemical reviews*, *119*(8), 5298-5415. https://doi.org/10.1021/acs.chemrev.8b00593

Yang, H., Gao, P. F., Wu, W. B., Yang, X. X., Zeng, Q. L., Li, C., & Huang, C. Z. (2014). Antibacterials loaded electrospun composite nanofibers: release profile and sustained antibacterial efficacy [10.1039/C3PY01335A]. *Polymer Chemistry*, *5*(6), 1965-1975. https://doi.org/10.1039/C3PY01335A

Yang, Q., Li, Z., Hong, Y., Zhao, Y., Qiu, S., Wang, C., & Wei, Y. (2004). Influence of solvents on the formation of ultrathin uniform poly(vinyl pyrrolidone) nanofibers with electrospinning [https://doi.org/10.1002/polb.20222]. *Journal of Polymer Science Part B: Polymer Physics*, *42*(20), 3721-3726. https://doi.org/https://doi.org/10.1002/polb.20222

Ye, Z., Xu, W., Shen, R., & Yan, Y. (2019). Emulsion electrospun PLA/calcium alginate nanofibers for periodontal tissue engineering. *Journal of Biomaterials Applications*, *34*(6), 763-777. https://doi.org/10.1177/0885328219873561

Yuan, X., Zhang, Y., Dong, C., & Sheng, J. (2004). Morphology of ultrafine polysulfone fibers prepared by electrospinning [https://doi.org/10.1002/pi.1538]. *Polymer International*, *53*(11), 1704-1710. https://doi.org/https://doi.org/10.1002/pi.1538

Zhao, H., & Chi, H. (2018). Electrospun Bead-on-String Fibers: Useless or Something of Value? In *Novel Aspects of Nanofibers*. https://doi.org/10.5772/intechopen.74661

Zong, X., Kim, K., Fang, D., Ran, S., Hsiao, B. S., & Chu, B. (2002). Structure and process relationship of electrospun bioabsorbable nanofiber membranes. *Polymer*,

43(16), 4403-4412. https://doi.org/https://doi.org/10.1016/S0032-3861(02)00275-6